Reaction-Driven Convection in a Porous Medium

William W. Farr, Jorge F. Gabitto, Dan Luss, and Vemuri Balakotaiah
Dept. of Chemical Engineering, University of Houston, Houston, TX 77204

The onset of three-dimensional reaction-driven convection in a porous medium is investigated using linear stability theory. The geometries investigated include a finite cylinder and a rectangular parallelepipped of arbitrary aspect ratios. The analysis determines, among other things, the likely modes (flow patterns) to emerge first as a function of reaction parameters and aspect ratios. The flow fields corresponding to three-dimensional modes are described in detail. Important qualitative differences are found between reaction-driven convection and the standard Lapwood or Bénard convection due to a temperature gradient applied to the boundaries of the system.

The second part of the work examines numerically reaction-driven natural convection in a porous two-dimensional rectangular box. Orthogonal collocation and continuation techniques are used to determine the conduction and convection branches of solutions as a function of the Rayleigh number (Ra), the Frank-Kamenetskii number (δ) and the aspect ratio (α). The convective solutions (streamlines and isotherms) corresponding to primary, secondary and tertiary bifurcations are presented. The effect of natural convection (Ra) on the ignition point (critical δ value) is determined for three different aspect ratios.

Part I: Linear Stability Analysis

W. W. Farr, J. F. Gabitto, D. Luss, and V. Balakotaiah

Introduction

The heat generated by a chemical reaction occurring in a porous medium creates density differences in the fluid and induces natural convection which, in turn, affects the rate of heat release by the reaction. The complex interaction between these two processes is the major cause of many instabilities observed in chemically reacting systems. This reaction-driven convection is also responsible for the delay of spontaneous ignition (thermal explosion) in coal piles, stored chemicals (such as organic peroxides and chlorates), grain, hay, biological, and waste dumps. In these cases, it is of interest to identify the conditions leading to the onset of natural convection and its influence on the critical conditions of self-ignition.

A substantial amount of work has been done on convective instabilities in porous media in which the driving force is a temperature gradient applied to the boundaries of the system (Lapwood, 1948; Davis, 1967; Gershuni and Zhukhovitskii, 1976; Beck, 1972; Kordylewskii et al., 1986). Many studies were concerned with convective instabilities in open systems (Nield, 1968; Homsy and Sherwood, 1976; Jones and Persichetti, 1986). Relatively few studies, however, appeared in the literature on reaction-driven convection. Jones (1973) determined the conditions for the onset of reaction-driven convection in a fluid confined between two infinite parallel plates. Kordylewski and Krajewski (1984) solved numerically the equations describing reaction-driven convection in a porous cylindrical container of equal height and diameter. They limited their analysis to solutions that are independent of the azimuthal angle to avoid lengthy numerical integration. More recently, Viljoen and Hlavacek (1987) studied numerically two-dimensional chemically-driven convection in a rectangle of

Correspondence concerning this article should be addressed to V. Balakotaiah.

fixed aspect ratio (length/height) as a function of the Frank-Kamenetskii parameter via a truncated Galerkin approximation.

In Part I of this article, we investigate systematically the onset of reaction-driven convection in a porous medium using linear stability theory. Our linear analysis results are quite general and considerably extend previous work on this problem. For example, we include three-dimensional disturbances, which have not been considered before, and show that under certain conditions they, and not two-dimensional modes, are the first disturbances to emerge. Also, we are able to obtain results for closed containers of arbitrary aspect ratios, while previous investigators considered only a single configuration. In particular, we consider cylindrical and three-dimensional rectangular containers of arbitrary aspect ratios and solve numerically the linear stability problem for various parameter values by a combination of separation of variables and the shooting method. We then specialize our results for comparison to those mentioned above. Special attention is paid to describing and visualizing the flow fields corresponding to the three-dimensional modes. We also compare the results of this study with the linear stability results of Lapwood or Bénard convection (Gershuni and Zhukhovitskii, 1976) and point out the differences between convection driven by a nonuniformly-distributed heat source (reaction-driven convection) and that due to a temperature gradient applied to the boundaries of the system.

In Part II of this work, we present a systematic numerical study of reaction-driven convection in a porous two-dimensional box. We use the orthogonal collocation and continuation techniques to determine the conduction and convective branches of solutions as a function of the Rayleigh number, the Frank-Kamenetskii number, and aspect ratio. We also present the flow patterns and isotherms corresponding to primary, secondary and tertiary convection branches. Finally, we determine numerically the effect of Rayleigh number on the ignition point for three different aspect ratios.

Model Equations

We begin by assuming that the Boussinesq approximation is valid and that Darcy's law describes the resistance to flow, and then make the usual assumption of a large Prandtl number. We assume that the pseudohomogeneous reaction is of order zero with an Arrhenius temperature dependence. The dimensionless energy, momentum, and continuity equations are:

$$\theta_t + v \cdot \nabla\theta = \Delta\theta + \delta \exp(X) \tag{1}$$

$$\nabla P = Ra\theta e_z - v \tag{2}$$

$$\nabla \cdot v = 0 \tag{3}$$

where

$$X = \frac{\gamma\theta}{(\gamma + \theta)} \tag{4}$$

and θ, P and v denote dimensionless temperature, pressure, and velocity, respectively, Ra is the Rayleigh number, γ is the dimensionless activation energy, and δ is the Frank-Kamenetskii parameter (proportional to the heat of reaction and reactant concentration). Explicit definitions are given in the Notation section. Boundary conditions on the top and bottom surfaces of the cylinder are

$$\theta(-1) = \theta(1) = 0 \tag{5}$$

while on the lateral surface,

$$\frac{\partial\theta}{\partial n} = 0 \tag{6}$$

i.e., insulated side walls. For the velocity, we require

$$v \cdot n = 0, \tag{7}$$

where n is the outward normal to the domain. For the rectangular box, we follow Viljoen and Hlavacek (1987) in prescribing Eq. 5 on the top surface and Eq. 6 on the bottom surface,

$$\theta_z(0) = \theta(1) = 0. \tag{8}$$

The domains, using dimensional variables, are shown in Figure 1. Note that h is half the height of the cylinder, so that $\eta = 1$ corresponds to the cylindrical configuration chosen by Kordylewski and Krajewski (1984) and $\alpha_1 = a/h = 2$ to the rectangular domain studied by Viljoen and Hlavacek (1987).

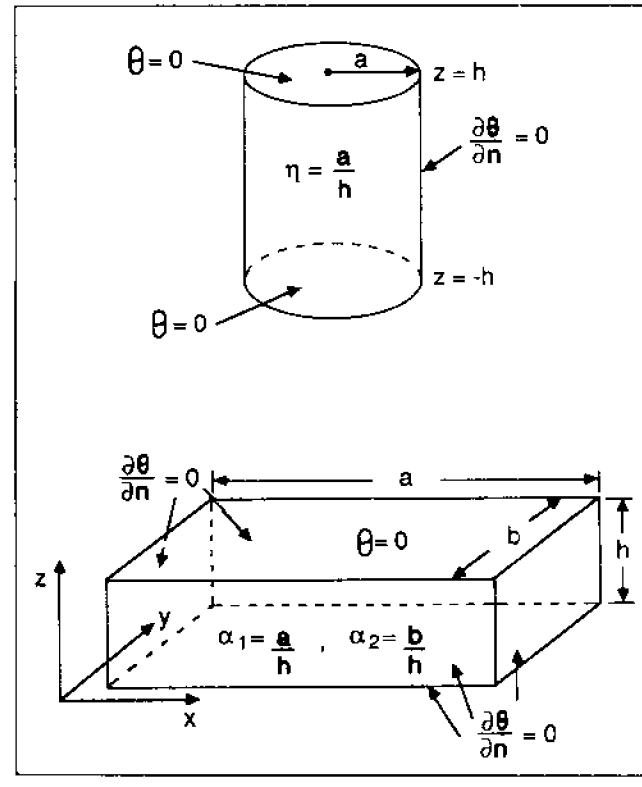

Figure 1. Domains and boundary conditions for the two geometries.

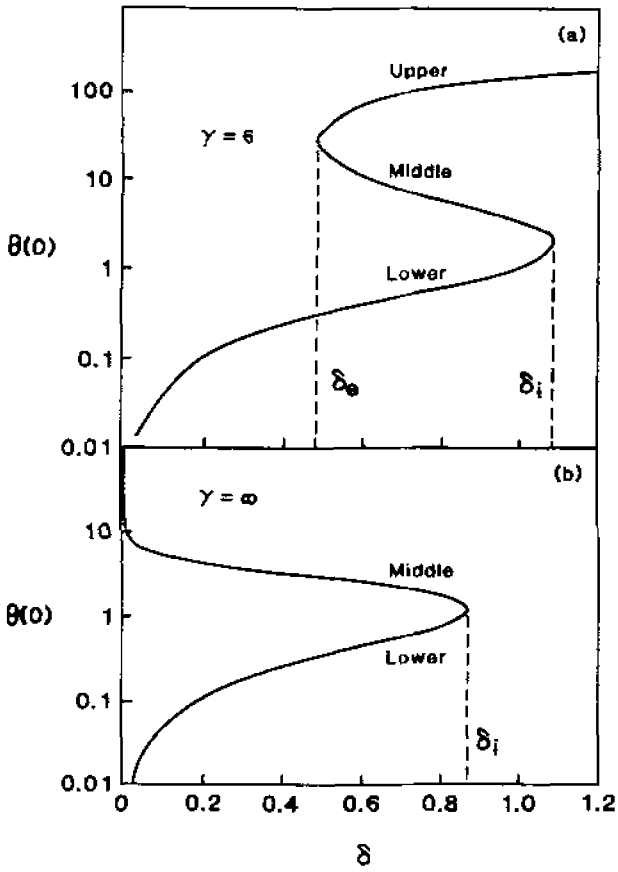

Figure 2. Bifurcation diagram of the conduction solution showing the upper, lower and middle branches: (a) for $\gamma = 6$ and (b) for $\gamma = \infty$.

The lateral boundary conditions are shown so that steady-state solutions exist for which $v = 0$. These conduction solutions depend only on the variable z and are obtained by solving

$$\theta_{zz} + \delta \exp(X) = 0 \tag{9}$$

with the boundary conditions Eq. 5 for the cylinder and Eq. 8 for the rectangular box. Solving these problems by the shooting method is straightforward. It should be noted that the solutions for the quiescent profiles in the cylinder and the box are really the same, since the solution of Eqs. 9 and 5 is symmetric about $z = 0$. Understanding these solutions will be important in our later development, so we describe them briefly. We consider only positive values of δ so that the profiles $\theta(z)$ for the cylinder are concave downward and have a single maximum at $z = 0$. Thus, the whole profile can be characterized by the value of θ at $z = 0$, and the solutions for different values of δ can be represented by a bifurcation diagram of $\theta(0)$ vs. δ. Using the positive exponential approximation (i.e., infinite γ), Eqs. 8-9 may be solved analytically (Frank-Kamenetskii, 1969) in a parametric form:

$$\theta(z) = 2 \ln\left(\frac{\operatorname{sech} cz}{\operatorname{sech} c}\right) \tag{10a}$$

$$\delta = 2c^2 \operatorname{sech}^2 c \quad (0 < c < \infty) \tag{10b}$$

The corresponding bifurcation diagram (Figure 2b) has a single limit point at $\delta_l = 0.8785$, $\theta(0) = 1.1869$ ($c = 1.1997$) and δ approaches 0 asymptotically for large values of $\theta(0)$. For finite, but large, γ, another limit point appears and the bifurcation diagram is the well-known S-shaped curve. Singularity theory may be used to show that the two limit points coalesce at the cusp point located at $\gamma = 4.069$, $\delta = 1.307$, and $\theta(0) = 4.897$. For γ values less than this, there is a unique conduction solution. For higher γ values, lower, middle and upper branches of steady-state solutions exist. The bifurcation diagram for $\gamma = 6$ is shown in Figure 2a and the three branches are identified. For larger values of γ, the upper limit point (extinction point) moves to very small values of δ and large values of $\theta(0)$.

The case $\gamma = 0$ corresponds to a uniform heat source and can be solved analytically. In this case, a unique temperature profile

$$\theta(z) = 0.5\delta(1 - z^2) \tag{11}$$

exists for each δ value and the bifurcation diagram of $\theta(0)$ vs. δ is a straight line of slope 0.5.

The linear stability (with respect to nonconvective disturbances which depend only on z) of these quiescent profiles is determined by the eigenvalues ζ of

$$\phi_{zz} + \delta F(z)\phi = \zeta\phi \tag{12}$$

with boundary conditions

$$\phi(-1) = \phi(1) = 0 \text{ (cylinder)} \tag{13a}$$

$$\phi_z(0) = \phi(1) = 0 \text{ (box)} \tag{13b}$$

and

$$F(z) = [\gamma/(\theta(z) + \gamma)]^2 \exp(X). \tag{14}$$

Equation 12 and either set of boundary conditions (Eq. 13) define a self-adjoint boundary value problem, so the eigenvalues are real and only a finite number can be positive (Coddington and Levinson, 1955). In fact, in this case, one eigenvalue is positive at most, which means that the upper branch is also stable. Note that for $\delta_\gamma = 0$, all the eigenvalues are negative, so the lower branch is stable. One might also wonder whether solutions with $v = 0$, but nontrivial spatial structure may bifurcate from these "trivial" profiles. It will be shown below that they can, but only from the middle branch, and hence are unstable next to the bifurcation point.

Linear Stability Analysis

We now consider the onset of natural convection by investigating the linear stability of these quiescent profiles. Disturbances Θ, Π, and U of the temperature, pressure and velocity must satisfy

$$\Theta_t + U \cdot H(z) e_z = \Delta\Theta + \delta F(z)\Theta \tag{15}$$

$$\nabla\Pi = Ra\Theta e_z - U \tag{16}$$

$$\nabla \cdot U = 0 \tag{17}$$

where

$$H(z) = d\theta(z)/dz. \tag{18}$$

By $\theta(z)$ we of course mean the solution to Eqs. 9 and 5 or Eq. 8. Boundary conditions for the perturbations are analogous to Eqs. 5, 6, 7 and 8.

We have stated above that we consider only positive values of δ. We also mainly consider positive values of Ra, but both of these assumptions are for convenience and historical precedent. Negative values of δ are possible if the reaction is endothermic instead of exothermic. In this case, however, no explosion can occur and it is of less intrinsic interest. Negative values of Ra can occur if the coefficient of temperature expansion, β, is negative. Intuitively, for convection to set in, the density should increase with increasing z in some part of the domain, i.e., $\beta\theta'(z) < 0$ for some value of z. Here, one must be careful to distinguish between the two examples chosen. For the cylinder, it is required that the boundary conditions are the same on the top and bottom and the quiescent profile be symmetric about $z = 0$. This means that the profile has both positive and negative temperature gradients. Thus, when the top and bottom boundary conditions are the same, the density is unstably stratified in some part of the domain regardless of the sign of β. It will be shown that for this symmetric case neutral stability to a particular form of disturbance at a positive Rayleigh number implies neutral stability to a related disturbance at minus that same value of Ra. The situation is quite different if either the top or the bottom is insulated, because the quiescent temperature profile is either monotonically increasing (top surface insulated) or monotonically decreasing (bottom surface insulated). We have chosen the second case for our illustration, for which intuition suggests that the upper and lower branches will always be stable if $Ra < 0$.

To solve Eqs. 13, 14, and 15 by separation of variables, we write

$$\Theta(x,y,z,t) = e^{\lambda t} f_0(x,y)\phi(z) \tag{19}$$

$$\Pi(x,y,z,t) = e^{\lambda t} h(x,y)p(z) \tag{20}$$

$$U(x,y,z,t) = e^{\lambda t}[f_1(x,y)u(z), f_2(x,y)v(z), f_3(x,y)w(z)], \tag{21}$$

substitute these expressions, and try to satisfy the equations and boundary conditions. For the cylinder we replace x and y with polar coordinates and define two operators that let us proceed in a coordinate-free way. The operators are Δ_2 and ∇_2, which are just the restrictions of Δ and ∇ to two dimensions. They satisfy the usual condition

$$\nabla_2 \cdot [\nabla_2 g(x,y)] = \Delta_2 g(x,y). \tag{22}$$

After some algebraic manipulations, it can be shown that separation of variables works if one can solve the eigenvalue problem

$$\Delta_2 h = -k^2 h, \quad \partial h/\partial n = 0 \tag{23}$$

on the lateral surfaces. Then, the functions f_0, f_1, f_2, f_3 are obtained from

$$f_0 = f_3 = h, \quad (f_1, f_2) = \nabla_2 h, \tag{24}$$

and the functions u, v, and p satisfy

$$u = v = -p = w'/k^2. \tag{25}$$

The only remaining functions are w and ϕ, which must satisfy

$$wH(z) = \phi'' - k^2\phi + [\delta F(z) - \lambda]\phi \tag{26}$$

$$w'' - k^2 w + k^2 Ra\phi = 0 \tag{27}$$

The boundary conditions for the cylinder (fixed temperature, top and bottom) are

$$w(-1) = w(1) = 0 \tag{28a}$$

$$\phi(-1) = \phi(1) = 0 \tag{28b}$$

while for the box we must use

$$w(0) = w(1) = 0 \tag{29a}$$

$$\phi'(0) = \phi(1) = 0. \tag{29b}$$

Before particularizing to one of the two geometries, we consider some special cases of Eqs. 26 and 27. First, we note that if $\delta = 0$ (no reaction), then $H(z) = 0$ and the equations decouple. It is simple to check that in this case all the eigenvalues λ are negative, so the quiescent solution is stable. If we set $Ra = 0$, then $w = 0$ and again the equations decouple. It is not much harder to check that again all of the eigenvalues λ are real and related to the eigenvalues of Eq. 12 by

$$\lambda = \zeta - k^2. \tag{30}$$

Thus, the eigenvalues λ are negative if the eigenvalues ζ are negative. A zero eigenvalue λ with $Ra = 0$ corresponds to a bifurcation to a solution with nontrivial spatial structure but $v = 0$. Equation 30 shows that such a bifurcation can occur only from the middle branch and hence must be unstable close to the point of bifurcation.

We note that for the case of uniform heat generation ($\gamma = 0$), $F(z) = 0$ and $H(z) = -\delta z$. In this case, Eqs. 26 and 27 take a simple form and the principle of exchange of stabilities can be proven, i.e., the eigenvalue problem is self-adjoint and the eigenvalues are real. For $\gamma = \infty$, the functions $F(z)$ and $H(z)$ can once again be determined explicitly:

$$\delta F(z) = 2c^2 \operatorname{sech}^2 cz \tag{31a}$$

$$H(z) = -2c \tanh cz \tag{31b}$$

For this case, or for the case of finite γ, the eigenvalue problem is not self-adjoint, and we have not been able to show that a Hopf bifurcation does not occur. The appearance of the function $F(z)$ makes the problem nonself-adjoint and prevents the

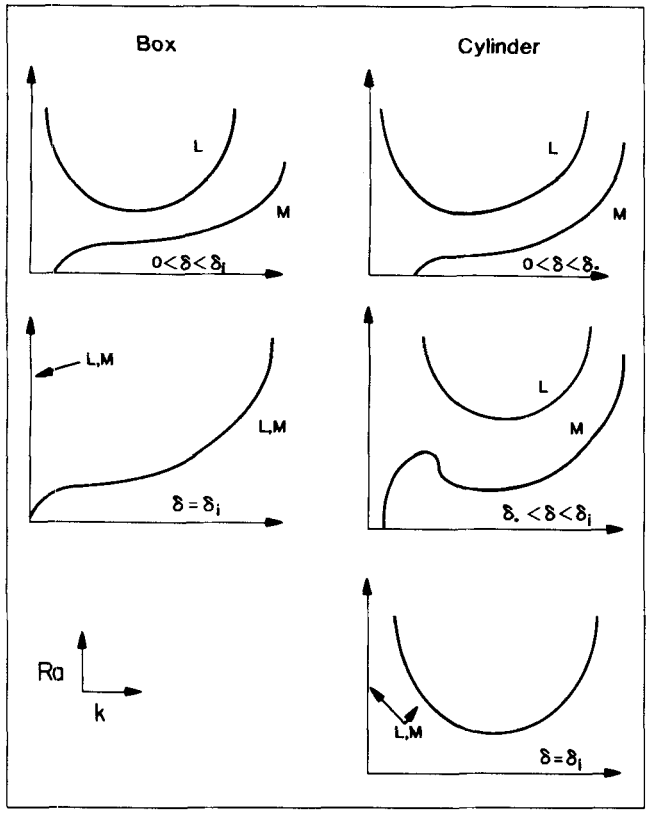

Figure 3. Neutral stability curves for the lower and middle branches of conduction solutions for $\gamma=\infty$.

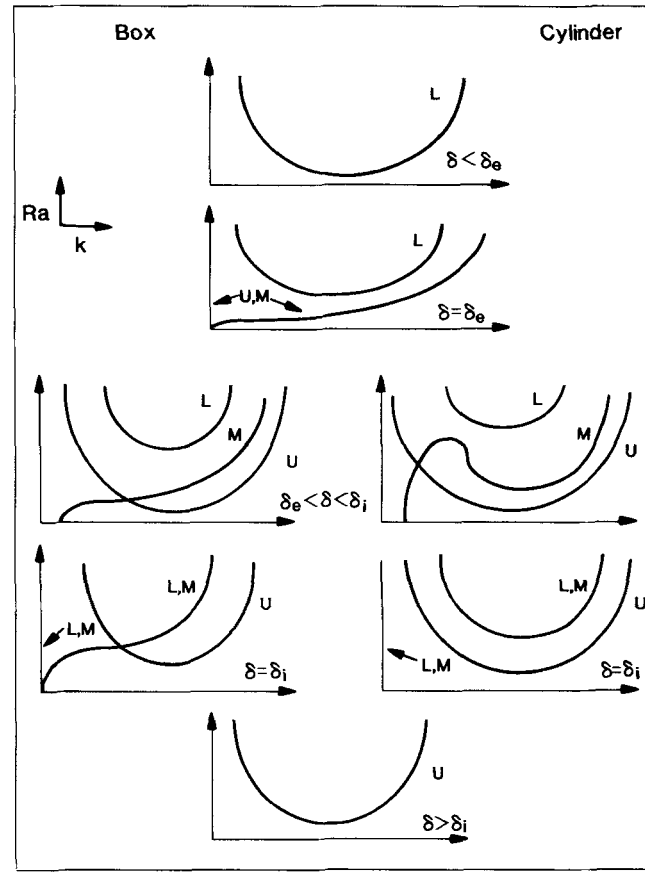

Figure 4. Neutral stability curves for the lower, middle and upper branches of conduction solutions for finite $\gamma>4.1$.

classical proof for Rayleigh-Benard convection from going through. It seems likely from the results above, however, that a Hopf bifurcation from the quiescent steady state will not be important for the "small" values of Ra. In any case, in this article we assume that a Hopf bifurcation does not occur and consider only solutions of Eqs. 26 and 27 with $\lambda=0$.

Equations 26 and 27 with $\lambda=0$ define a boundary value problem for which a nontrivial solution exists only if a certain condition depending on Ra, k, γ and δ is satisfied. It is convenient to combine the two equations into a single fourth-order equation in w

$$w^{(IV)}-[2k^2-\delta F(z)]w''+[k^4-k^2\{\delta F(z)-RaH(z)\}]w=0, \quad (32)$$

where w must satisfy the boundary conditions

$$w(-1)=w''(-1)=w(1)=w''(1)=0 \quad (33)$$

for the cylinder. Since θ is an even function of z, H is an odd function of z. Thus, if Eqs. 32 and 33 are satisfied by $w(z)$, k, Ra, δ, and γ, they are also satisfied by $w(-z)$, k, $-Ra$, δ, and γ. This verifies the claim made above that for the cylinder neutral stability to a particular disturbance at a positive Rayleigh number implies neutral stability to a related disturbance at minus the same Rayleigh number. For the box, Eq. 33 must be replaced with

$$w(0)=w'''(0)-k^2w'(0)=w(1)=w''(1)=0. \quad (34)$$

Note that by replacing z by $1-z$ the solution for a box insulated on the bottom can be used to determine neutral stability for a box which is isothermal on the bottom and insulated on the top, but this will not be pursued here.

Setting $k=0$ in Eq. 32 gives,

$$w^{(IV)}+\delta F(z)w''=0. \quad (35)$$

If we let $\chi(z)=w''(z)$, then χ satisfies Eq. 12 with $\zeta=0$. This means that at a limit point of the quiescent solution, we have neutral stability with $k=0$ for any value of Ra. It also implies that Eq. 32 has no nontrivial solution for $k=0$ except at a limit point of the quiescent solution.

We solved Eq. 32 by the shooting method, treating this boundary value problem as an initial value problem by guessing the initial conditions at the lower boundary and trying to satisfy the boundary conditions at $z=1$. Note that for the case of finite γ, we must integrate Eq. 9 simultaneously, and so require a starting value for it as well. Two of the four required initial conditions for Eq. 32 come from Eq. 33 or 34 and linearity allows us to set $w'=1$, so we need only specify $w'''(-1)$ (cylinder) or $w''(0)$ (box). Three conditions (Eqs. 5, 33 or 34) are to be satisfied at $z=1$, so another variable must be specified. We chose Ra for the third unknown, and solved for the two

unknown conditions at the lower boundary and Ra as functions of k for several fixed values of δ and γ. Note that for each value of δ in the region of multiple steady states, there are three different choices for the functions $F(z)$ and $H(z)$ corresponding to the three different branches of solutions to Eq. 9.

The results of the calculations in Figures 3 and 4 show the different types of neutral stability curves that are possible for different values of γ and δ. It should be pointed out that referring to the curves in Figures 3 and 4 as being for the box and the cylinder is convenient but somewhat misleading. It follows from the separation of variables treatment above that *these results are not specific to any cross-sectional geometry: they depend only on the top and bottom boundary conditions.* Thus, the results in Figures 3 and 4 can also be applied to compare a box (or a cylinder) which is insulated on the bottom to one which is twice as high but whose bottom temperature is fixed.

Figure 3 shows that for $\gamma=\infty$, there are two branches of the neutral stability curve for all $\delta<\delta_i$ (ignition point). These correspond to the lower and middle branches of the quiescent solutions shown in Figure 2b. As expected, the neutral stability curve for the middle branch crosses the k axis at the positive value. This curve is found to be monotonic for the box, but for the cylinder it has a maximum and a minimum for some range of δ values ($\delta_*<\delta<\delta_i$ where $\delta_*=0.747$ and $\delta_i=0.8785$). It was reasoned above that at a limit point of the quiescent solutions, the entire Ra axis is a part of the neutral stability curve. Numerical calculations in Figure 3 verify this and also show that there is another curve in the positive quadrant of the (Ra,k) plane. On this curve, bifurcation to a convection solution coincides exactly with a limit point of the quiescent solution. Numerical calculations have shown that this curve is monotonic with k for the case of a box but has a local minimum ($Ra=17.34$ at $k=1.7$) for the case of a cylinder. The interpretation of the result for the box is that for any $\delta<\delta_i$ there is a critical Rayleigh number (Ra_c) such that for all $Ra<Ra_c$ the lower conduction branch is stable while for $Ra>Ra_c$ it is unstable to disturbances having wave numbers in a range $k_1<k<k_2$. As δ approaches δ_i, both Ra_c and k_1 approach zero. Thus, when the density is unstably stratified, long wavelength convection is possible for arbitrarily small values of Ra provided δ values are close to δ_i. In contrast, for fixed temperature boundary conditions where the density is stably stratified in the lower half and unstably stratified in the upper half, the lower conduction branch becomes unstable to convective disturbances (of finite wavelength), only if the Rayleigh number exceeds a certain minimum value (17.34). This value is determined by the temperature profile corresponding to the ignition point (Eq. 10a with $c=1.1997$).

Figure 4 shows the types of neutral stability curves that are possible for finite values of the activation energy $\gamma>4.1$. For $\delta<\delta_e$ (extinction point), there is a single neutral stability curve corresponding to the lower branch of quiescent solutions. At the extinction point, the Ra axis is a part of this curve. In addition, there is another monotonic curve (for the box as well as the cylinder) that passes through the origin. This result implies that long wavelength convection is possible for very small values of the Rayleigh number for both types of boundary conditions, provided that the conduction solution is in the ignited state and δ values are close to the extinction point. For

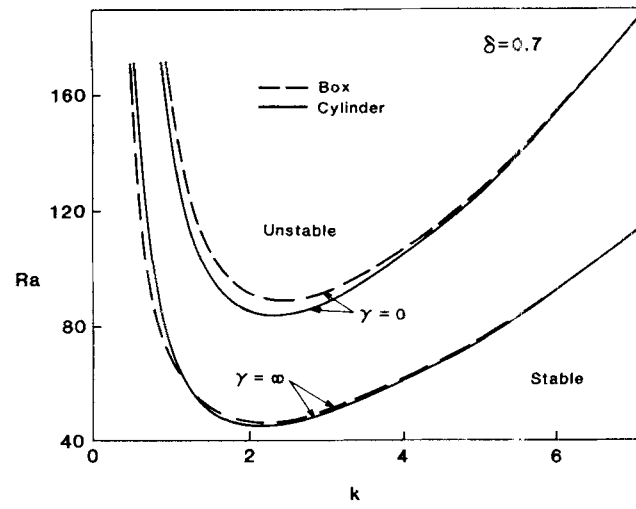

Figure 5. Numerically-computed neutral stability curves for the lower conduction solution for $\delta=0.7$ and $\gamma=0, \infty$.

The first vertical mode is destabilized above the respective curve.

all δ values in the region (δ_e, δ_i), the neutral stability curve consists of three branches. The middle branch is once again found to be monotonic for the box but for fixed temperature boundary conditions it may have two extrema for δ values close to δ_i. At $\delta=\delta_i$, the lower and middle branches coalesce, and for all $\delta>\delta_i$ there is a single branch of the neutral stability curve corresponding to the ignited conduction branch.

Figure 5 shows the exact numerically-computed neutral stability curve for the lower branch of quiescent solutions for $\delta=0.7$ and two different values of γ. These calculations indicate that for the δ values far away from the ignition point, the neutral stability curves for the box and the cylinder are very close to each other. This is due mainly to defining Ra and δ using half the cylinder height, but the full height of the box. This was done on purpose to make the temperature gradients in the unstably stratified parts (i.e., $z>0$ for $Ra>0$) of the quiescent profiles equal for the two cases. The idea behind this is that convective instabilities are due primarily to the gradients in the fluid density, which for a Boussinesq fluid are linearly related to the temperature gradient. Thus, it is not surprising that the curves are close to each other. Numerical computations have shown that for the case of uniform heat generation ($\gamma=0$), the values of the Rayleigh number are slightly lower for the cylinder. However, for all $\gamma>4.1$, the two curves intersect and the box has lower values of Ra for small k. For intermediate values of the wave number the cylinder has slightly lower Ra values, while at high k values the two curves practically coincide. The deviation between the two types of boundary conditions becomes more prominent as δ approaches δ_i (ignition point). The neutral stability curves for this case are shown in Figure 6. Intuitively, one can see that the class of disturbances that can destabilize the conductive state of the box is a subset of that for the cylinder. However, Figure 6 shows that the cylinder has a larger critical Ra value at all k values. This behavior is caused by the nonmonotonic behavior of the neutral stability curve of the unstable conduction branch for fixed temperature boundary conditions. It is due to the stable stratification of the density in the lower half of the cylinder. It is not possible to have fluid motion in the upper

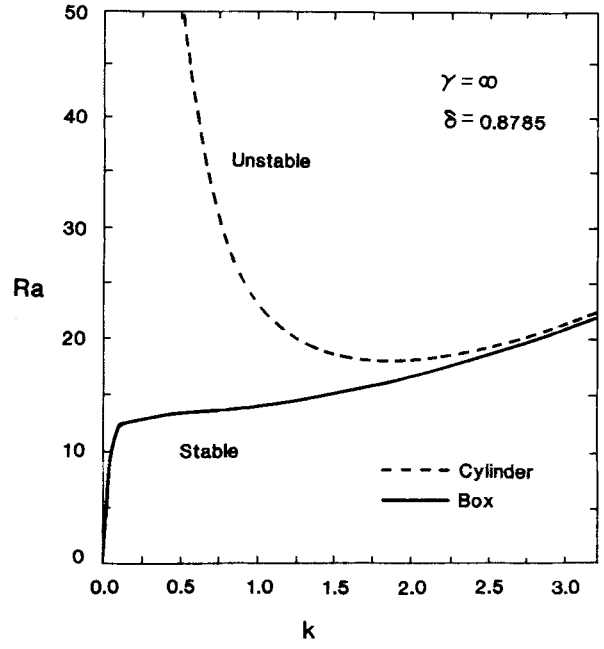

Figure 6. Neutral stability curves for the lower branch of quiescent solution at the limit point.

The *Ra* axis is also a part of the neutral stability curve.

half without having motion also in the lower half. Thus, a higher driving force is needed to cause convective motion in the cylinder than in the box.

To contrast the two different cases, we compared eigenfunctions $w(z)$ for the two sets of boundary conditions with parameter values $\delta = 0.7$, $\gamma = \infty$, and $k = 2$ and 3. The eigenfunction for the box (insulated bottom case) is found to be very similar in shape to $\sin(\pi z)$, but is skewed slightly; the maximum occurs just past $z = 1/2$. The eigenfunction for the cylinder (fixed bottom temperature) is found to be skewed in a more dramatic fashion. This probably reflects on the region

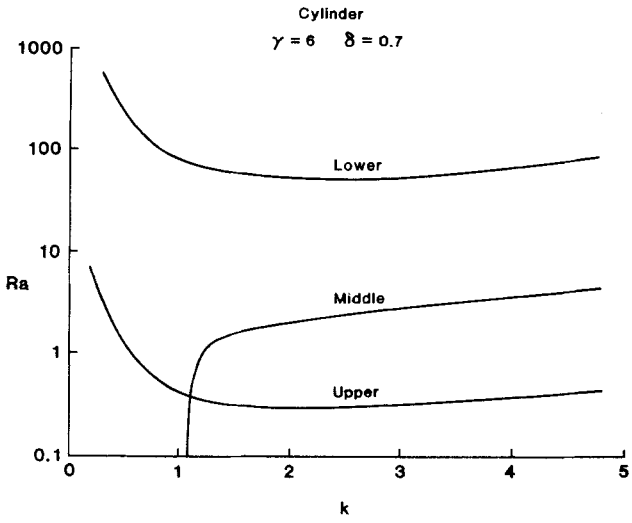

Figure 7. Neutral stability curves for cylindrical geometry for all the three branches of quiescent steady states.

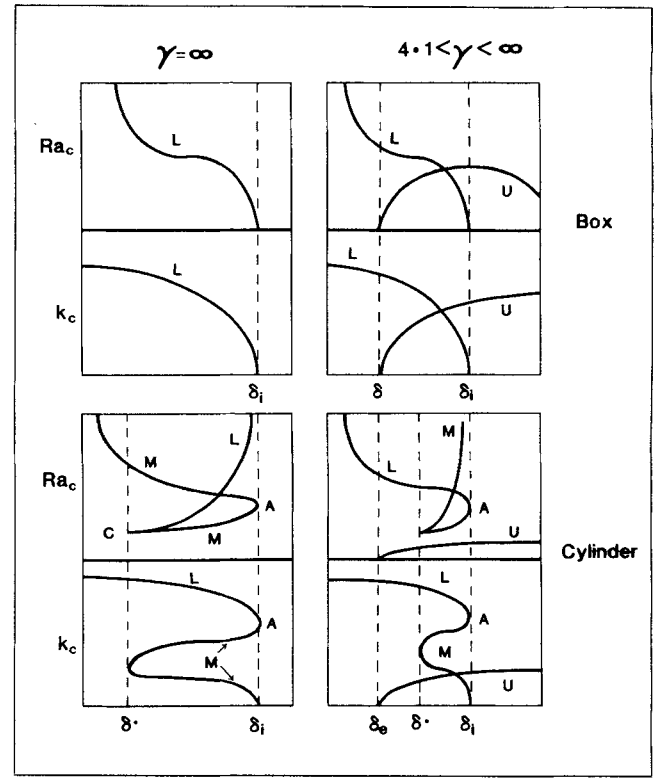

Figure 8. Dependence of the critical Rayleigh number, (Ra_{min} or Ra_{max}) and wave number on the Frank-Kamenetskii parameter.

$z \geq 0$ being unstably stratified for the quiescent solution, but there is a significant tail of the eigenfunction for negative values of z. This tail means that while the convective motion will be most intense in the top half of the cylinder, significant fluid motion will also occur in the lower region. We use this observation later to describe the expected flow patterns, but since our description is qualitative in nature we will only need to recall that the eigenfunctions have a single interior maximum and no interior zeros.

Figure 7 shows the exact numerically-computed neutral stability curves for all three branches of quiescent solutions for fixed-temperature boundary conditions. The small γ value of 6 keeps the value of *Ra* on the upper branch from becoming very small, but the qualitative results are unchanged for larger γ values. The neutral stability curve for the lower branch is very similar to the one for $\gamma = \infty$ in Figure 5. The corresponding curves for the upper and middle branches appear at much smaller values of the Rayleigh number, with the one for the upper branch similar in appearance to the one for the lower branch. The small Rayleigh numbers can be rationalized on physical grounds if we recall from Figure 2a that the quiescent profiles on the upper branch contain rather steep temperature gradients. These results are to be interpreted only in a qualitative way as the Boussinesq approximation may not be valid on the upper branch.

Figure 8 shows the critical Rayleigh number, Ra_c, and the wave number, k_c (corresponding to the maxima or minima in Figures 3 and 4) as a function of the Frank-Kamenestkii parameter δ. The exact numerically-computed curves for the lower

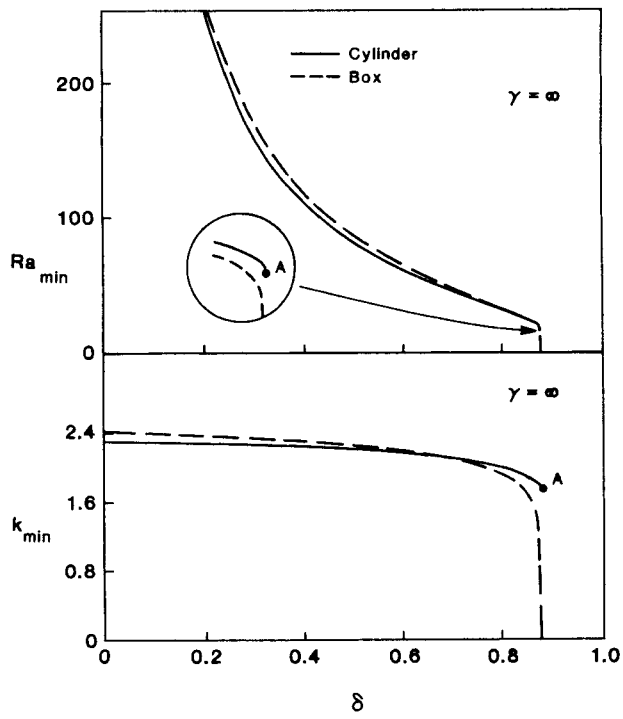

Figure 9. Numerically-computed curves of dependence of the critical Rayleigh number and wave number on the Frank-Kamenetskii parameter for the lower branch of quiescent solutions.

branch of quiescent solution are shown in Figure 9 for $\gamma=\infty$. These curves may be used to determine the smallest value of the Rayleigh number for the onset of convective motion on the lower branch of Figure 2b. As expected, $Ra_{\min}$ for the box decreases monotonically from infinity to zero as δ increases from zero to δ_i. For the cylinder, $Ra_{\min}$ decreases from infinity ($\delta=0$) to 17.34 ($\delta=\delta_i$). Thus, for the case of fixed-temperature boundary conditions, convective motion may exist only if Ra exceeds a critical value. In contrast, for the insulated bottom boundary condition, convection could set in for arbitrarily small values of the Rayleigh number provided that the aspect ratios are small and δ value is close to that of the ignition point.

It is interesting to compare the above results for the onset of convection due to a distributed heat source with that of Lapwood convection. The latter is described by Eq. 32 with $F(z)=0$, $H(z)=1$ and the boundary conditions $w(0)=w(1)=w''(0)=w''(1)=0$. The neutral stability curve for this case is given by Lapwood (1948) and Gershuni and Zhukhovitskii (1976):

$$\hat{Ra}=\frac{(N^2\pi^2+k^2)^2}{k^2}, \tag{36}$$

where N is the vertical mode number. The smallest value of $\hat{Ra}$ is obtained for $N=1$, $k=\pi$ and $\hat{Ra}_c=4\pi^2\approx 39.5$. $\hat{Ra}$ is related to Ra by:

$$\hat{Ra}=\frac{Ra\gamma(\Delta T)}{T_o} \tag{37a}$$

$$=Ra\theta(0). \tag{37b}$$

For the case of a uniform heat source, $\theta(0)=0.5\,\delta$, and from Figure 5 we see that $(Ra\,\delta/2)_c=31$ (box) and 29.5 (cylinder). Thus, the critical $\hat{Ra}$ values for a uniform heat source are only about 25% lower than that for the Lapwood problem with the same ΔT. However, for the case of an Arrhenius heat source, $\hat{Ra}$ approaches zero for a box and is about 50% lower for a cylinder.

It follows from Eq. 36 that for $k\to 0$ the neutral stability curve for the Lapwood convection approaches the curve asymptotically

$$\hat{Ra}=\frac{N^4\pi^4}{k^2} \tag{38a}$$

while for $k\to\infty$, it approaches the curve

$$\hat{Ra}=k^2. \tag{38b}$$

Asymptotic analysis of Eq. 32 for $k\to\infty$ shows that the neutral stability curve for $\gamma=\infty$ approaches the curve

$$Ra=\frac{k^2}{4cI(N)} \tag{39}$$

where

$$I(N)=\begin{cases}\displaystyle\int_0^1 \sin^2 N\pi z\,\tanh\, czdz & \text{(box)}\\ \displaystyle\int_0^1 \sin N\pi z\cos\left\{(2N-1)\frac{\pi z}{2}\right\}\tanh\, czdz & \text{(cylinder)}\end{cases}$$

The integral $I(N)$ is a weakly decreasing function of the vertical mode number N. Thus, in contrast to Eq. 36, the neutral stability curves of Eq. 32 for different modes intersect at high k values. This result is confirmed numerically in Figures 10 and 11. This result implies that for small aspect ratios (height much larger than lateral dimensions) the higher vertical modes are destabilized first.

The above comparison and the results in Figures 3-11 clearly show that the behavior of reaction-driven convection is markedly different from that of Lapwood or Bénard convection.

Convective Modes in a Box

We consider a box, insulated on the bottom, of height h with two aspect ratios: α_1 for the x direction and α_2 for the y direction. Using the derivation above and the standard eigenfunctions for the two-dimensional Laplacian with Neumann boundary conditions, the disturbance eigenfunctions can be obtained as:

$$U\cdot e_x=\frac{-n\pi}{\alpha_1}w_N'(z)\sin\left(\frac{n\pi x}{\alpha_1}\right)\cos\left(\frac{m\pi y}{\alpha_2}\right) \tag{40a}$$

$$U\cdot e_y=\frac{-m\pi}{\alpha_2}w_N'(z)\cos\left(\frac{n\pi x}{\alpha_1}\right)\sin\left(\frac{m\pi y}{\alpha_2}\right) \tag{40b}$$

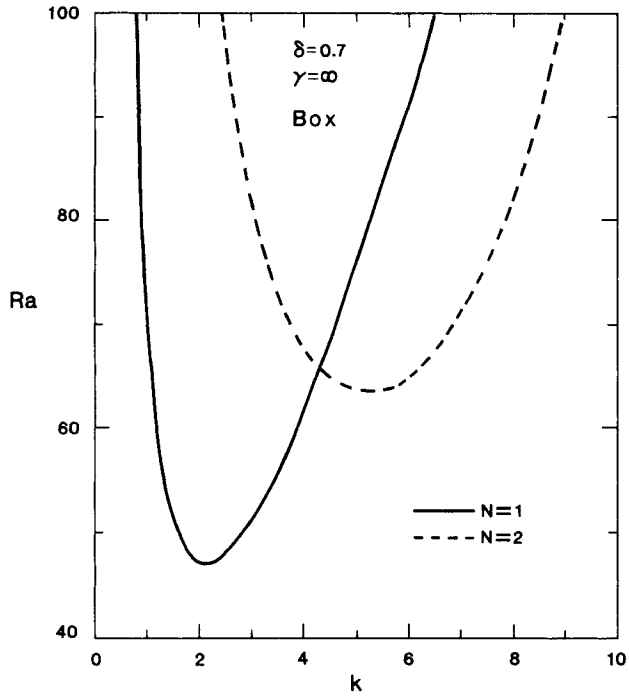

Figure 10. Neutral stability curves for the lower branch of quiescent solutions for the first two vertical modes ($N=1, 2$) in rectangular geometry.

$$U\cdot e_z=\left[\left(\frac{n\pi}{\alpha_1}\right)^2+\left(\frac{m\pi}{\alpha_2}\right)^2\right]w_N(z)\cos\left(\frac{n\pi x}{\alpha_1}\right)\cos\left(\frac{m\pi y}{\alpha_2}\right) \tag{40c}$$

$$\Theta=\left[\left(\frac{n\pi}{\alpha_1}\right)^2+\left(\frac{m\pi}{\alpha_2}\right)^2\right]\phi(z)\cos\left(\frac{n\pi x}{\alpha_1}\right)\cos\left(\frac{m\pi y}{\alpha_2}\right) \tag{40d}$$

where w_N and ϕ satisfy Eqs. 27 and 32 with

$$k^2=\left(\frac{n\pi}{\alpha_1}\right)^2+\left(\frac{m\pi}{\alpha_2}\right)^2 \tag{40e}$$

Setting $m=0$ gives two-dimensional results, that is, rolls with axes parallel to the y axis. Similarly, setting $n=0$ gives rolls with axes parallel to the x axis.

We speak of values of N, m and n as defining modes, since they describe how the solutions of the nonlinear equation will look close to the bifurcation point. Now suppose that we want to determine the value of Ra for the neutral stability of the quiescent solution on the lower branch, say, at some fixed value of δ for the various modes. Then, for the fixed values of α_1 and α_2, we can compute a value for k from Eq. 40e for each set (N,m,n) and then use results like those in Figure 3 or 10 to determine a value of Ra. The most dangerous mode is defined as the one for which Ra is minimized, since it is the first to become unstable as Ra is increased. To simplify the discussion, we assume $N=1$ in the rest of this section and write $w(z)$ for $w_1(z)$.

Determining how the most dangerous mode depends on the aspect ratios α_1 and α_2 is a difficult and complex task and we do not intend to complete fully that here. Some insight can be gained, however, from the following considerations, leading to conditions on α_1 and α_2, which guarantee that the most dangerous mode is two-dimensional. Suppose that one wants to know the most dangerous mode for specific values of α_1 and α_2. Clearly, one wants the value of k obtained from Eq. 40e to be as close as possible to k_{min}, that is the minimum value of k on the Ra vs. k curve. This suggests that we can get a crude idea of the most dangerous mode by using k_{min} in Eq. 40e and solving for α_1 and α_2 for various values of n and m. We present a qualitative version of this procedure for the first few modes ($n,m\leq 3$) in Figure 12. The pure-mode cases for which either n or m is zero are shown as a vertical ($m=0$) or

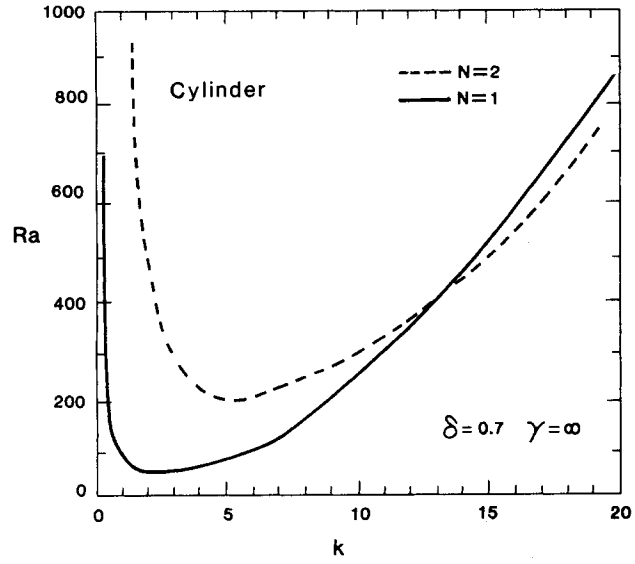

Figure 11. Neutral stability curves for the lower branch of quiescent solutions for the first two vertical modes ($N=1, 2$) in cylindrical geometry.

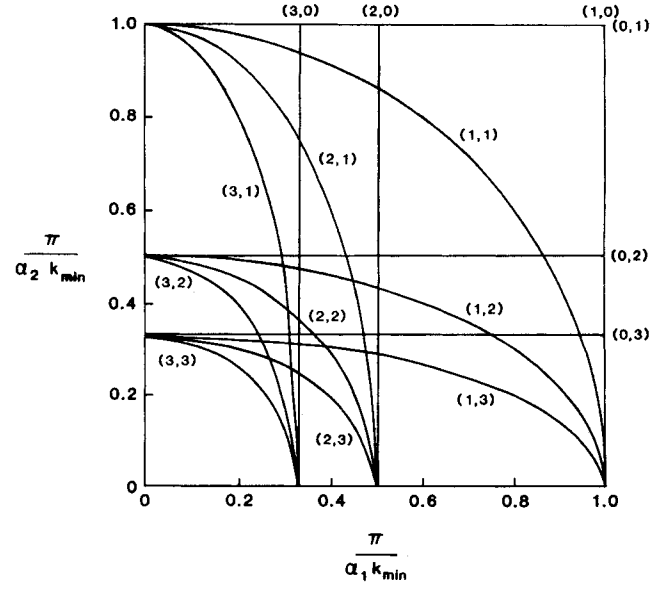

Figure 12. Solutions of Eq. 40e with $k=k_{min}$ for various values m and n.

horizontal ($n=0$) line. The mixed-mode cases for which neither n or m is zero are represented either as a circle ($m=n$) or an ellipse ($m \neq n$), restricted to the first quadrant.

To plot the neutral stability surface for any particular mode (i.e., for fixed values of m and n) we would have to add a third dimension to Figure 12 for the value of Ra. For the pure modes with $m=0$, the neutral stability surface for a particular point on the lower branch of quiescent solutions is swept out by translating the two-dimensional result (e.g., Figure 5) parallel to the α_2 axis and similarly for the pure modes with $n=0$. For the mixed modes, the shape of the neutral stability surface for a particular mode can be visualized by imagining the surface swept out by translating the two-dimensional result along the portion of the ellipse in the first quadrant corresponding to the mode; but, if $n \neq m$, there must also be a deformation along with the translation. The neutral stability surface is then the lower envelope of the neutral stability surfaces of all of the modes. As can be imagined, this surface becomes quite complicated. An example of such a surface for a simpler problem is described by Beck (1972). The important feature for our purposes, however, is that the curves for the mixed modes in Figure 12 are all contained inside the box $0 \leq (1/\alpha_1) \leq k_{\min}/\pi$, $0 \leq (1/\alpha_2) \leq k_{\min}/\pi$. This is also true for all the higher mixed modes not shown in Figure 10. From Figure 9 we see that the largest value of $k_{\min}$ is about 2.4. Thus, if α_1 and α_2 are smaller than 1.3, the pure modes will be the most dangerous. Further, if we have $\alpha_2 << \alpha_1$ (that is the x side is much longer than the y side), the most dangerous modes will be rolls with axes parallel to the y axis, as expected.

It is difficult to get a good idea of how the flow corresponding to the three-dimensional modes looks like. The pure modes are the familiar convection rolls, since for the two-dimensional mode $n \neq 0$, $m=0$ a stream function, Ψ, is given by:

$$\Psi = \sin\left(\frac{n\pi x}{\alpha_1}\right) w(z). \tag{41}$$

The level curves of Eq. 41 give the streamlines for this pure mode; and given the behavior of $w(z)$, it is clear that rolls are obtained. If m and n are both nonzero, a stream function cannot be obtained, but it turns out that the generalization

$$\Psi(x,y,z) = \sin\left(\frac{n\pi x}{\alpha_1}\right) \sin\left(\frac{m\pi y}{\alpha_2}\right) w(z) \tag{42}$$

of Eq. 41 has the property

$$\nabla\Psi \cdot U = 0 \tag{43}$$

where U is as in Eq. 40. Streamlines for U are integral curves of the vector field whose right-hand side is U, so the level surfaces of Eq. 42 have the property that any streamline that starts on a particular level surface stays on that level surface for all time. If we consider first $m=n=1$, then it is not too hard to see how the level surfaces of Eq. 42 inside the box of Figure 1 look like. The surface $\Psi=0$ gives the surface of the box, while the maximum value that Ψ can attain (equal to the maximum value of w) gives a single point approximately at the center of the box. An intermediate value of Ψ gives a surface lying inside the box that looks like a distorted sphere. Now

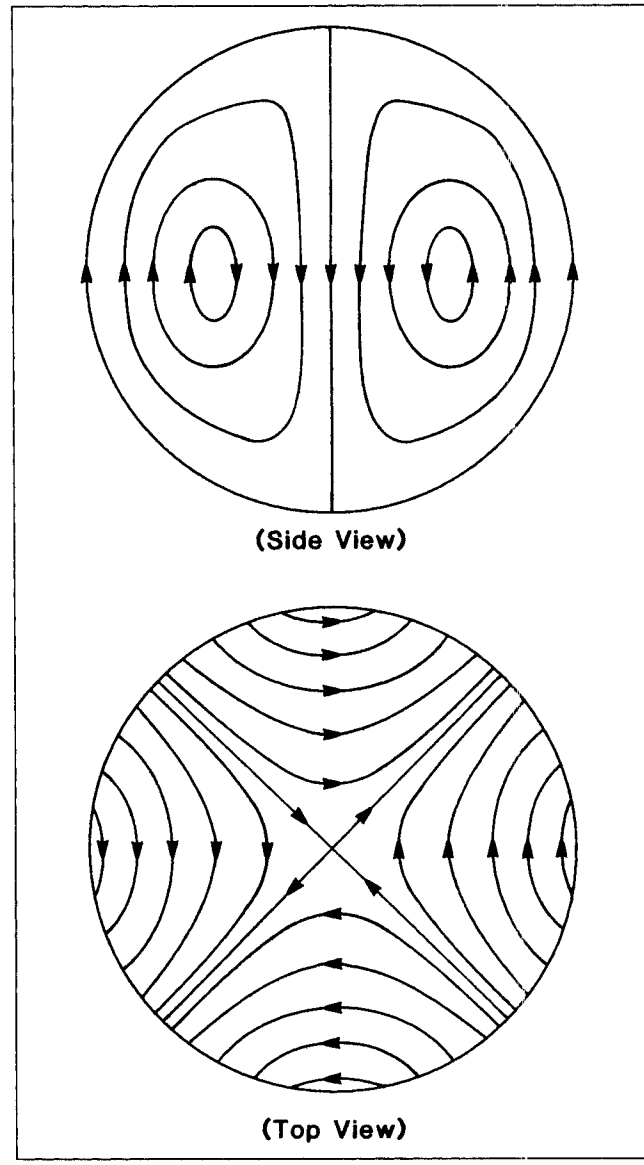

Figure 13. Flow patterns on a stream surface for modes $n=1$ and $m=1$ (rectangular geometry): top and side view of half of a sphere.

consider the three lines parallel to the coordinate axes which pass through the single point where $\Psi = \Psi_{\max}$. It is easy to check that these three lines give the only solutions to $U=0$. The intersection of these three lines with a distorted sphere gives six points: the North and South poles and the four points of the compass on the equator. These six points are the only steady states on the level surface of the vector field whose integral curves are the streamlines we seek. Using phase-plane techniques at each steady state, we find that the poles are saddles and the four points on the equator are centers. Hence, the streamlines are as in Figure 13, showing half of the sphere. By combining the flow patterns on the stream surfaces, we see that the box contains four convective cells. Generalizing to other nonzero values of n and m is straightforward. We just form $n \cdot m$ subboxes: the streamlines in each subbox are like

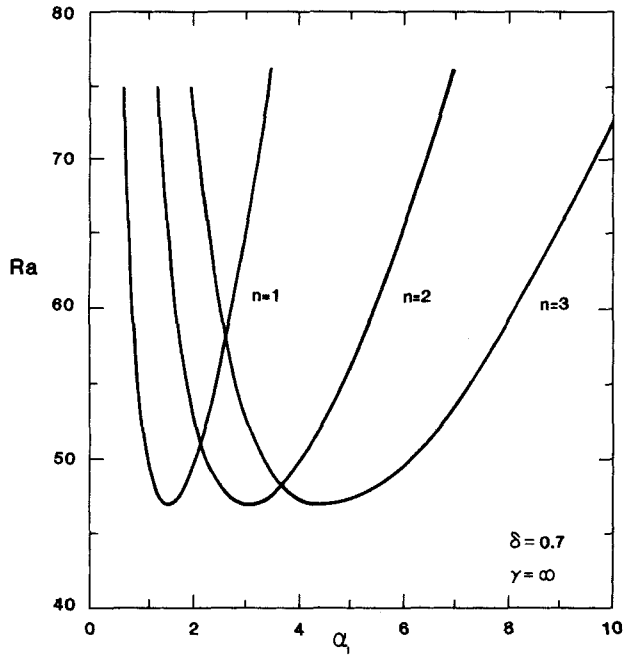

Figure 14. Neutral stability curves for the lower branch of quiescent solutions for horizontal modes $n=1, 2, 3$ in a rectangular geometry.

those for $m=n=1$, except that the directions of flow alternate from box to box.

To compare our results to those of Viljoen and Hlavacek (1987) and with the numerical calculations in Part II we now consider only the pure modes with $m=0$. Our discussion above shows that this is equivalent to assuming α_2 small, that is, the width of the box in the y direction is smaller than its height. If we make that assumption on α_2, it is not difficult to determine the most dangerous mode for any value of α_1. We merely use Eq. 40e (with $m=0$) to relate k to α_1 for each fixed value of n. We have plotted the neutral stability curves for the lower branch vs. α_1 for the first few modes in Figure 14, using the results in Figure 5. Changing the value of δ on the lower branch has the same effect as it did previously, since the curves in Figure 12 are obtained in a simple way from the corresponding curve in Figure 5.

The neutral stability boundary is, of course, made up of the lower envelope of the curves for all the values of n. The physical interpretation of Figure 14 is that for each value of α_1 there is a most dangerous mode, or at special values of α_1 two modes n and $n+1$ are the most dangerous simultaneously. These latter points are known as multicritical points or mode interactions, and are the topics of current research (e.g., Golubitsky et al., 1988; Dangelmayr and Armbruster, 1986; Armbruster et al., 1988). The surprising fact about mode interactions is that solutions of unexpected type can appear: for example, periodic solutions in the interaction of two steady-state modes.

Due to the simplicity of Eq. 40e and the shape of the Ra vs. k curve, we can make some useful generalizations. In the first place, the neutral stability boundary is made up of segments of the neutral stability curves for each n, and the value of n changes at a multicritical point involving modes n and $n+1$. It is also clear that, due to the shape of the Ra vs. k curve, multicritical points can never involve more than two modes. This is not true if we do not restrict ourselves to two-dimensional modes. Mode interactions involving three modes are possible then. Thus, the location of these multicritical points is of great interest. To be more precise, we introduce some notation. The Ra vs. k curve has a single minimum at a point which depends only on the parameters δ and γ; we will denote this point by $(k_{\min}, Ra_{\min})$. Then, the bicritical point involving modes n and $n+1$ is obtained by locating the two points on the $Ra(k)$ curve and the unique value of α_1 which satisfy

$$Ra\left(\frac{n\pi}{\alpha_1}\right) = Ra\left(\frac{(n+1)\pi}{\alpha_1}\right) \equiv Ra_n \tag{44}$$

where we require

$$\frac{n\pi}{\alpha_1} < k_{\min} < \frac{(n+1)\pi}{\alpha_1} \tag{45}$$

From Eq. 45, it follows that

$$k_{\min}/(n+1) < \pi/\alpha_1 < k_{\min}/n. \tag{46}$$

Hence, the value of α_1 for the bicritical point involving modes n and $n+1$ can be approximated by:

$$1/\alpha_{1,n} = \frac{k_{\min}}{2\pi}\left[\frac{1}{n} + \frac{1}{(n+1)}\right] \tag{47}$$

For $\delta=0.7$ and $\gamma=\infty$ ($k_{\min}\approx 2.1$), Eq. 47 predicts $\alpha_{1,1}=2$ and $\alpha_{1,2}=3.57$. The corresponding numerically-computed values are 2.08 and 3.57.

To extend our results to the upper and middle branches, it is convenient to fix the value of α_1 and plot the neutral stability curve for specific modes as δ varies. This method of presenting the results is useful, because it shows how the bifurcation point for a particular convective mode moves around on the bifurcation diagram of the quiescent steady states as Ra is varied. We now compare our results for $\alpha_1=2$ to those of Viljoen and Hlavacek (1987) and to the numerical calculations in Part II. Figure 15 shows the portions of the curves for modes $n=1$ and $n=2$ corresponding to the lower branch and part of the middle branch. The interpretation is that for large values of Ra, the bifurcation points to convection solutions are located on the lower branch of quiescent solutions, and as Ra is decreased the convection solution bifurcation points pass through the limit point of the quiescent solutions at $\delta=0.8785$ and onto the middle branch. Eventually, the bifurcation points move onto the upper branch, though this is not shown in the figure. (In our discussion of the cylinder we will present similar curves for finite γ which include all three branches of Figure 2a.) Note that a portion of the $n=1$ curve corresponding to the middle branch shown in the figure has negative values of Ra. Also, at $\delta\approx 0.56$ corresponding to the lower branch of quiescent solutions we see a bicritical point involving modes 1 and 2. That such a point exists for $\alpha_1=2$ was obvious from Figure 14, which also told us that the two important modes on the lower branch are $n=1$ and $n=2$. The figure shows that at $\delta=0.8785$ the bifurcation point to a convection solution exactly

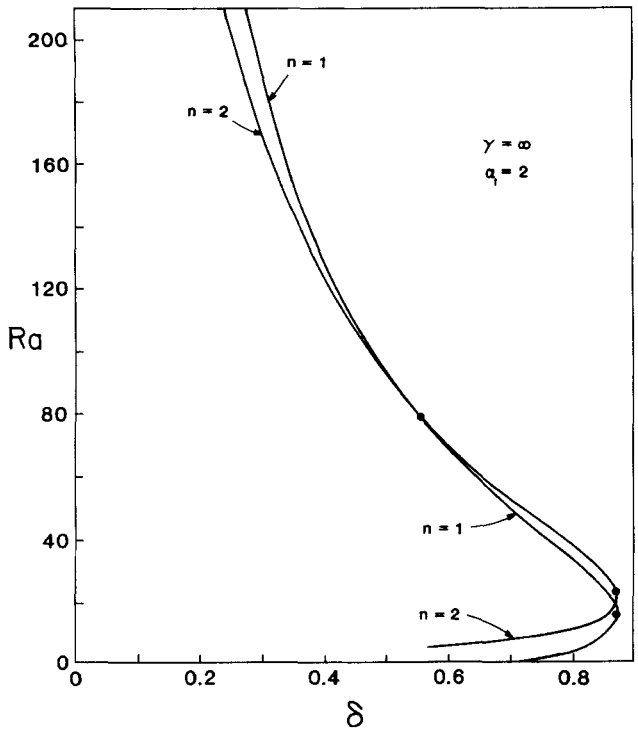

Figure 15. Neutral stability curves, *Ra* vs. δ, with positive exponential approximation and $\alpha_1 = 2.0$ for horizontal modes $n = 1$ and $n = 2$ in a rectangular geometry.

coincides with a limit point of the quiescent solution. These points may also be thought of as bicritical points; they determine the critical value of Rayleigh number (Ra_c) at which the lower conduction branch of Figure 2 begins to lose stability. Figure 6 may be used to determine Ra_c for any aspect ratio. The above analysis implies that the $Ra < Ra_c$, the entire lower conduction branch is stable to convective disturbances and the system will not ignite up to the conduction limit ($\delta_{ig} = 0.8785$ for $\gamma = \infty$). For $Ra > Ra_c$, a part of the conduction branch loses stability and convection pushes the ignition point to higher values of δ. The numerical calculation of this ignition locus is presented in Part II.

Because Viljoen and Hlavacek (1987) used the width, instead of the height, for their characteristic length, their parameter *FK* is four times our parameter δ and their Rayleigh number is twice ours (for $\alpha_1 = 2$). Their results for $Ra = 30$ and $Ra = 50$, correspond to ours for $Ra = 15$ and $Ra = 25$. Since we have performed only the linear stability analysis we can only compare the locations of the $n = 1$ and $n = 2$ bifurcation points. The agreement is rather good, considering the approximations made by Viljoen and Hlavacek (1987). At $Ra = 15$, they found a mode $n = 1$ bifurcation point on the lower branch, we find it on the middle branch. That is, they predict that convection would set in and increase the region of thermal stability, but our calculations show that this is not the case. However, a change of 10–20% in the value of *Ra*, which is consistent with the level of approximation they used, would move the mode $n = 1$ bifurcation point onto the lower branch in agreement with their results. The same order of approximation holds for $Ra = 25$. The more accurate numerical calculations in Part II show good agreement with the results of this section.

Convective Modes in a Finite Cylinder

We consider a cylinder as in Figure 1, with fixed and equal temperatures at the top and bottom and insulated sides. The disturbance eigenfunctions, in accordance with our development above, are given by

$$U \cdot e_r = kJ_m'(kr) w_N'(z)/k^2 e^{im\Psi} \tag{48}$$

$$U \cdot e_\Psi = imJ_m(kr) w_N'(z) e^{im\Psi}/(rk^2) \tag{49}$$

$$U \cdot e_z = J_m(kr) w_N(z) e^{im\Psi} \tag{50}$$

$$\Theta = J_m(kr)\phi(z) e^{im\Psi} \tag{51}$$

where $J_m (m \geq 0)$ is the mth Bessel function, and the parameter k is determined by the boundary conditions on the lateral surface to be

$$k = \frac{k_{nm}}{\eta} \tag{52}$$

where k_{nm} is the nth root of J_m'. The functions w_N and θ satisfy Eqs. 26 and 27 with boundary conditions given in Eq. 28. We will consider here only the case of $N = 1$. If $m > 0$ we note that the eigenfunction can be split into independent real and imaginary parts. This means that the eigenvalues are double, except when $m = 0$, and is a consequence of the cylindrical symmetry (periodic boundary conditions). Below, when we describe how the eigenmodes look like, we will describe the consequences of symmetry in more detail. Because the real and imaginary parts can be related by a phase shift, we only consider the real part in our investigations.

This problem would seem, at first glance, to be simpler than the box since there is only one aspect ratio. Determining the most dangerous mode, however, is complicated by the fact that there are still two integers, m and n, to contend with and also that there is no analytic way to determine the k_{nm}. Tabulated values of k_{nm} for $0 \leq m \leq 8$ and $1 \leq n \leq 20$ appear in Abramowitz and Stegun (1965). Using Eq. 52 we can generate a neutral stability curve for the fixed values of m and n, obtained simply by shifting the curve in Figure 5 and plotting $1/\eta$ vs. *Ra*. These are shown in Figure 16 for $n = 1$ and $m = 0$, 1, 2. If we are interested in the values of η close to 1, the most dangerous mode is $m = 1$. As before, the physical interpretation of Figure 16 is that for each value of η there is a most dangerous mode, to which the quiescent solution becomes unstable at the lowest value of *Ra*. Kordylewski and Krajewski's (1984) results are for $\eta = 1$, for which the most dangerous mode is $m = 1$ followed by $m = 2$ and $m = 0$. Because they considered only $m = 0$ modes, their results for small Biot numbers (we are treating only $Bi = 0$) are probably not physically meaningful. That is, the solutions they determined (to be stable) are not stable to three-dimensional perturbations, and hence their results are probably not useful. Furthermore, results for the related problem of imposed temperature-gradient-driven free convection in cylinders, reported in Gershuni and Zhukovitskii (1976), indicate that as $Bi \to \infty$, modes $m = 2$ and $m = 0$ change their relative positions, but $m = 1$, $n = 1$ is still the most dangerous mode. We conjecture that a similar situation holds for the present problem.

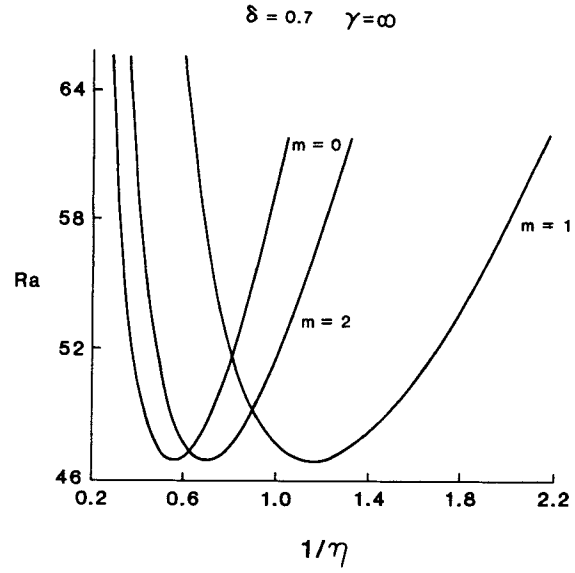

Figure 16. Neutral stability curves for the lower branch of quiescent solutions for modes $n=1$ (radial) and $m=0, 1, 2$ (azimuthal) in cylindrical geometry.

Also of interest in Figure 16 are the bicritical points where two modes are simultaneously most dangerous. Analyses of these interactions by Dangelmayr and Armbruster (1986) and Armbruster et al. (1988) have produced surprisingly complicated results. For example, under certain conditions the $m=1$, $m=2$ steady-state mode interaction can produce two different types of periodic solutions as secondary bifurcations, as well as quasiperiodic solutions as tertiary bifurcations.

Determining what the flow corresponding to the eigenfunctions (Eqs. 52-55) looks like is the easiest for $m=0$. Then, the solutions are rotationally-symmetric and two-dimensional. A stream function is given by

$$\Psi = -rkJ_0'(kr)\ w(z)/k^2 \tag{53}$$

and the contours of Ψ for $n=1$ give the results of Figure 1 in Kordylewski and Krajewski (1984). The convection cells resemble tori for $n=1$ and concentric cells for $n>1$. If $m>0$, no stream function exists, but as for the rectangular case we can find a function Ψ, given by

$$\Psi(r,\psi,z) = rJ_m'(kr)\sin(m\psi)\ w(z) \tag{54}$$

which satisfies Eq. 43 for the real part of U from Eqs. 48-50, that is, the streamlines all lie on the level surfaces of Ψ. To visualize the flow, we first consider $m=1$, $n=1$. Since J_1' then has no interior zeros, the level surfaces of Eq. 54 are qualitatively similar to those of Eq. 42 except that ψ can vary from 0 to 2π. Thus, we get two distorted spheres, one on each side of the plane $\psi=0$. The surface $\Psi=0$ gives this plane and the entire surface of the cylinder, while the maximum and minimum values of Ψ each give a single point. The only solutions of Real $(U)=0$ are the lines $\psi=\pm\pi/2$ and $z=z_{max}$, where z_{max} is the unique zero of $w'(z)$. These lines intersect each distorted sphere in exactly two points, which can be shown to be centers.

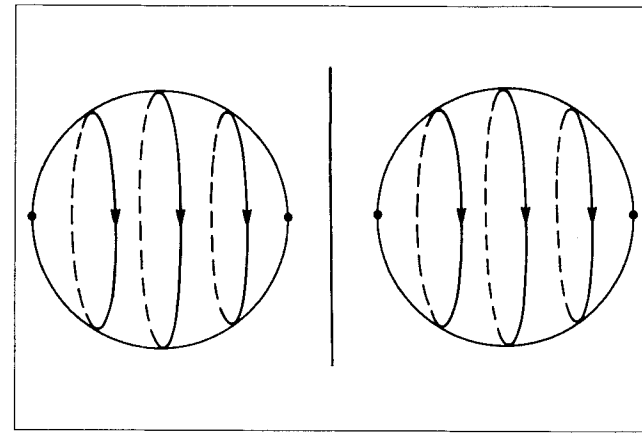

Figure 17. Flow patterns of a stream surface for modes $n=1$ and $m=1$ (cylindrical geometry).

Thus, the streamlines on the two spheres must be as in Figure 17. Increasing the value of n produces more spheres in the radial direction, while increasing m gives more spheres in the azimuthal direction. As in the box, the direction of flow alternates, but we must be a little careful about what we mean by this in the case of cells in the azimuthal direction. The precise statement is that if we take the real part of Eqs. 48-51 and change ψ to $\psi+(\pi/m)$, we obtain a minus sign multiplying each component.

As a final result, we show in Figure 18 the neutral stability curves, Ra vs. δ, for a cylinder with $\eta=1$ for the modes $n=1$ and $m=1, 2$ for all the three branches of quiescent solutions. One might wonder why the middle and upper branches are included since any branch that bifurcates from the middle branch is unstable near the point of bifurcation and the assumption of zeroeth-order kinetics (no reactant consumption)

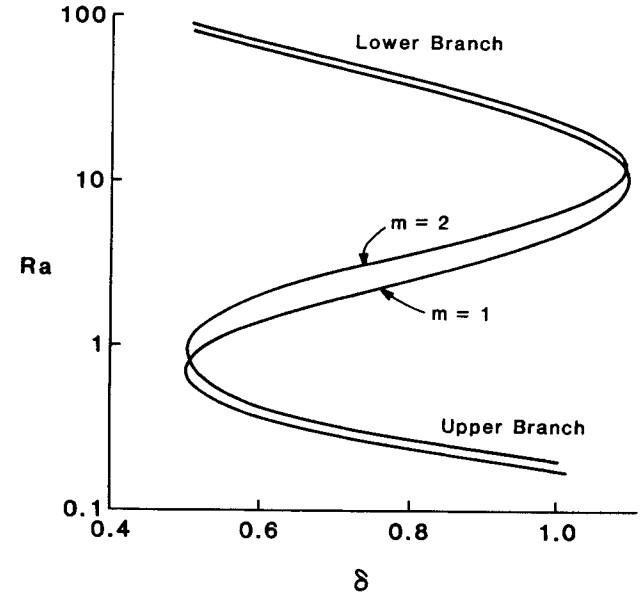

Figure 18. Neutral stability, Ra vs. δ, for cylindrical geometry with $\eta=1$, $\gamma=6$ and modes $n=1$ and $m=1, 2$.

is no longer valid on the upper branch. Our answer is that including them ties together the results, as we now demonstrate. If we fix $\eta = 1$, then by fixing $k = k^*_{nm}$ we can track a particular mode as δ is varied. In Figure 18 we show the plots of Ra vs. δ for mode $n=1$, $m=1$ (the most dangerous mode) and, for comparison, mode $n=1$, $m=2$. Consider first the $m=1$ mode. We determined above that for $Ra=0$, the upper and lower branches are stable. As Ra is increased, a bifurcation point for mode 1 appears on the upper branch at large values of δ and moves toward the upper limit point. At $Ra \approx 0.7$, the bifurcation point passes through the limit point, at which point the entire upper branch becomes unstable to convective disturbances. The lower branch remains stable until $Ra = 10$, when the bifurcation point has traversed the entire middle branch and emerges from the lower limit point. As stated above, mode $m=1$, $n=1$ is always the most dangerous mode, but we have also included mode $m=2$, $n=1$ in Figure 18 to give some indication of the complications that can arise in this model. Other modes could be included in the figure, but they would not change the pattern.

Part II: Numerical Bifurcation Analysis

J. F. Gabitto and V. Balakotaiah

Introduction

In the second part of this work we present a comprehensive numerical study of reaction driven convection in a porous two dimensional rectangular box. Using the streamfunction formulation, the governing equations can be written as

$$\Delta_2 \Psi + Ra \frac{\partial \theta}{\partial x} = 0 \tag{55}$$

$$\frac{\partial \theta}{\partial t} = \Delta_2 \theta - \frac{\partial \Psi}{\partial x}\frac{\partial \theta}{\partial z} + \frac{\partial \Psi}{\partial z}\frac{\partial \theta}{\partial x} + \delta \exp(\theta), \qquad (0<z<1,\ 0<x<\alpha_1) \tag{56}$$

The corresponding boundary conditions are,

$$\Psi = 0; \quad x = 0,\ \alpha_1 \tag{57a}$$

$$\Psi = 0; \quad z = 0,\ 1 \tag{57b}$$

$$\frac{\partial \theta}{\partial x} = 0; \quad x = 0,\ \alpha_1 \tag{57c}$$

$$\frac{\partial \theta}{\partial z} = 0; \quad z = 0; \tag{57d}$$

$$\theta = 0; \quad z = 1. \tag{57e}$$

A two-dimensional box has only one aspect ratio, α_1. So, in what follows we drop subscript 1 from the aspect ratio.

In Part I of this work, we examined the stability of the lower conduction solution to convective disturbances and determined the critical Rayleigh number (Ra_c) above which the lower conduction branch becomes unstable. The smallest value of Ra_c occurs at $\delta = \delta_{ig}$ implying that the lower conduction solution is destabilized first at the limit point. The dependence of Ra_c on the aspect ratio was shown in Figure 6 (where $k = \pi/\alpha$). For (Ra,k) values below this curve, the entire lower conduction branch is stable to convective disturbances and the system either ignites or jumps to a stable convective solution (if it exists) at $\delta_{ig} = 0.8785$. For (Ra,k) values above the curve, convective solutions exist and extend the ignition limit to higher values of δ. The type of convective solution that emerges first may be characterized by the number of cells (rolls) in the horizontal and vertical directions. Linear stability results may be used to show that the number of cells in the vertical direction is always one at $\delta = \delta_{ig}$. However, for $\delta < \delta_{ig}$, it may exceed one but this occurs only at small aspect ratios ($\alpha < 1$). In this work, we restrict our computations to the case of $\alpha > 1$. We refer to solutions having m-horizontal cells as a mode m solution.

Numerical Method and Accuracy of Computations

The system given by Eqs. 55-57 is solved using the orthogonal collocation method with cosine functions as the orthogonal trial functions. The stream function (Ψ) and temperature θ are approximated by,

$$\Psi = x(\alpha - x)\, z \sum_{i=1}^{M}\sum_{j=1}^{N} A_{ij} \cos\left\{\frac{\pi(2i-1)z}{2}\right\} \cos\left\{\frac{\pi(j-1)x}{\alpha}\right\} \tag{58}$$

$$\theta = \sum_{i=1}^{M}\sum_{j=1}^{N} B_{ij} \cos\left\{\frac{\pi(2i-1)z}{2}\right\} \cos\left\{\frac{\pi(j-1)x}{\alpha}\right\} \tag{59}$$

When Eqs. 58-59 are substituted into Eqs. 55-56 and the residual is set to zero at the $M \times N$ collocation points {located at the zeros of $\cos[\pi(2M+1)z/2]$ and $\cos[\pi(N+1)x/\alpha]$}, a system of $M \times N$ linear algebraic equations and $M \times N$ first-order differential equations is obtained. The linear equations may be solved for A_{ij} in terms of B_{ij} and Ra, and the result may be substituted into the differential equations. This procedure reduces Eqs. 55-56 into a set of $M \times N$ differential equations for the coefficient B_{ij} and simplifies the stability calculations.

In the study of thermal convection, it is customary to choose Ra as the distinguished bifurcation parameter. The reason is that the Ra number is a linear function of the applied temperature gradient and in thermal convection experiments this quantity is easily controlled. In reaction-driven convection studies, it is more convenient to use the Frank-Kamenetskii parameter (δ) as the bifurcation parameter (Jones, 1973; Viljoen and Hlavacek, 1987). The use of Ra number as a bifurcation parameter allows one to study more easily the bifurcating branches close to the conduction solution and the interaction among branches. The use of δ as a distinguished parameter, on the other hand, is more suitable to study the stability, because the amount of convective movement (Ra) is kept fixed while the amount of heat generated is increased (δ) and the conduction solution is only a function of the bifurcation parameter (δ). In this work, calculations using both Ra and δ as bifurcation parameter will be presented.

The different branches of solutions are computed using a continuation algorithm similar to the one presented by Kubicek and Marek (1983). In the case when Ra is the bifurcation parameter, the procedure described above to calculate the A_{ij} coefficients as a function of the B_{ij} coefficients and Ra number is used at every step of the calculations. When δ is the bifurcation parameter, this is not necessary because the relation between A_{ij} and B_{ij} is given by a constant matrix. The stability of the solutions is calculated by evaluation of the eigenvalues of the Jacobian matrix of the equations resulting from the application of the procedure described above. The terms of the Jacobian are numerically evaluated. The results obtained by the numerical evaluation are compared against derivatives evaluated algebraically in the few cases where this is possible to check the accuracy of the results. The numerical and algebraic results agreed within a 5% error.

The number of points used in the calculations is important from a quantitative as well as a qualitative point of view. Studies have been reported (Viljoen and Hlavacek, 1987; Gatica et al., 1989) where approximations using only one point in the z direction have been used. These approximations can lead to incorrect results even from a qualitative point of view because the use of cosines as basis functions for the temperature expansion forces the system to have a maximum on the bottom part of the domain. The results obtained in this study show that the coefficients B_{2j} corresponding to the second basis function $[\cos(3\pi z/2)]$ have a numerical value that is only about 10% of the value of the coefficients (B_{1j}) corresponding to the first basis function $[\cos(\pi z/2)]$, but the inclusion of the second (and higher order) basis functions in the z direction produces a displacement of the hot spots in the isotherm plots. This effect can be seen in Figure 19 and is important in understanding the behavior of the system.

Most of our calculations are done using three or more points in the vertical direction (z) and six or more in the horizontal direction (x). The influence of the number of points in both directions is shown in Figure 20 for a primary branch of positive mode 2 solution. These results are typical of all our calculations and show that the use of more points in either direction is not necessary to compute the primary convective solutions. In the case of secondary and tertiary convective branches, a higher-order approximation is needed.

Hopf bifurcations were found in some of the calculations done in this work when lower-order approximations were used.

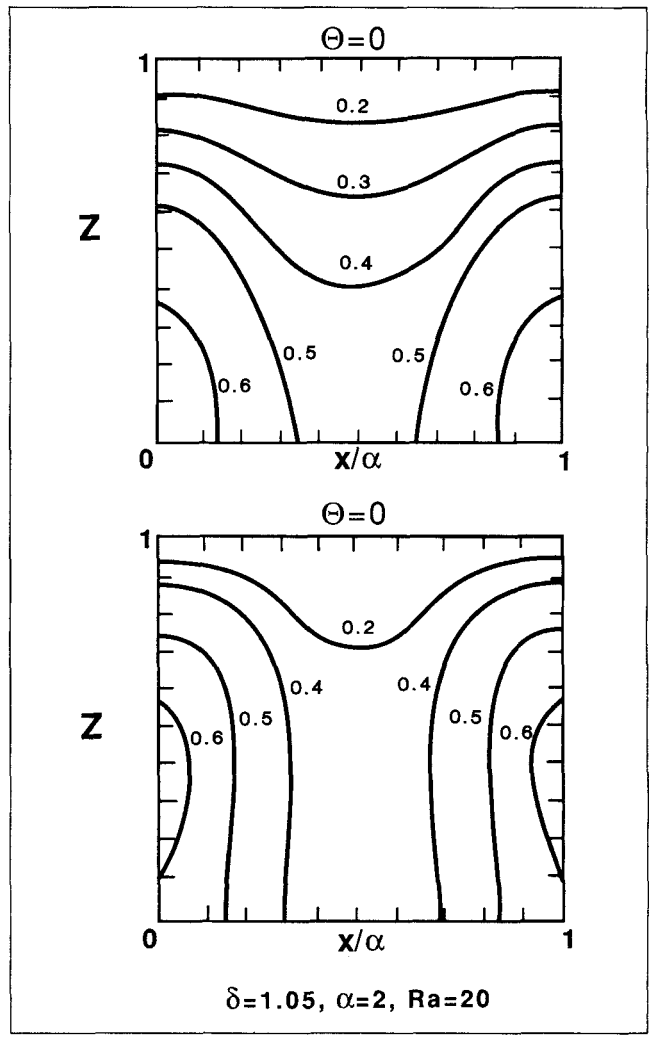

Figure 19. Influence of number of basis functions (N) in z-direction on the isotherms.

Top diagram, $N=1$; bottom diagram, $N\geq 2$

Most of them disappeared when the number of terms was increased. The Hopf bifurcations that did not disappear with increase in the number of points are related to branches bifurcating from the middle part of the conduction solution. Viljoen and Hlavacek (1987) reported the presence of Hopf bifurcation points for branches bifurcating from the lower conduction solution. We believe that their results are due to the lower-order approximation they used. We show in Figure 21 the conduction and convection branches for a lower-order approximation (as used by Viljoen and Hlavacek, 1987) and a higher-order approximation used in this work. This comparison clearly shows that the lower-order approximation used by Viljoen and Hlavacek (1987) does not capture even the qualitative bifurcation picture. A series of calculations using the Galerkin approximation scheme presented by Viljoen and Hlavacek (1987) were done. The idea was to compare the results obtained by both methods. To explore the accuracy of these results, computations with more terms in the Galerkin approximations for streamlines and temperature, were done. Using low-order approximations, we were able to reproduce their

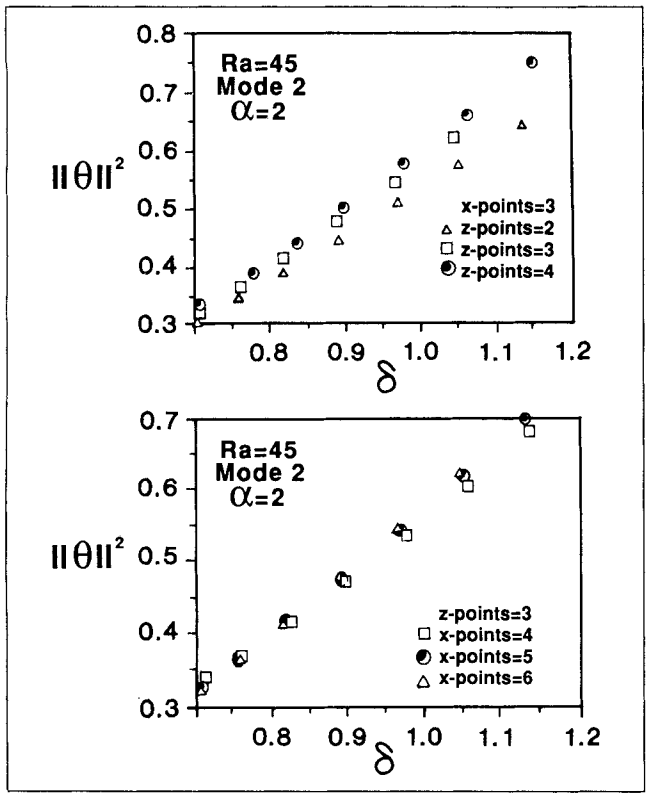

Figure 20. Influence of number of collocation points on the numerical results.

results. But, for higher-order approximations, qualitative differences as shown in Figure 21 appeared. It is also found that the bifurcation diagrams computed by the Galerkin and collocation methods agreed satisfactorily when compared at the same level of approximation.

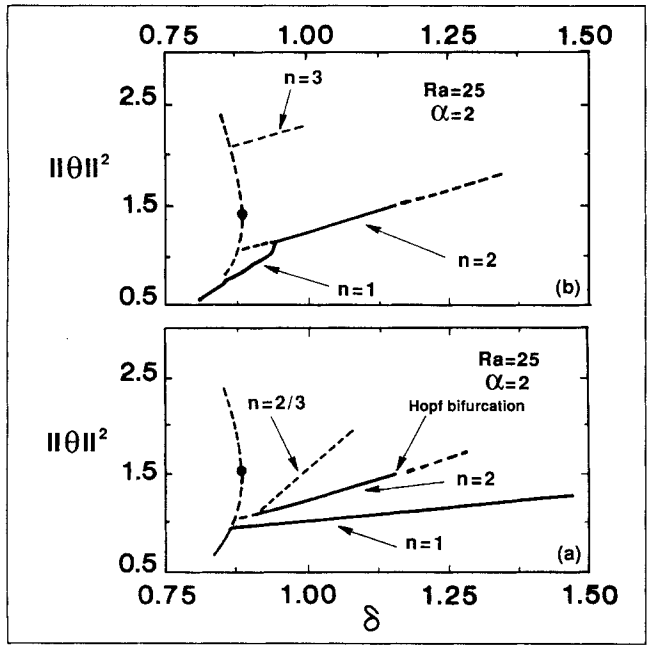

Figure 21. Bifurcation diagrams computed by: (a) lower-order and (b) higher-order Galerkin approximation methods (• limit point).

The accuracy of our calculations was also checked by comparing the values of *Ra* number for the crossing of primary convective branches through the limit point of the conduction solution with the exact values determined by linear stability analysis. This comparison in Table 1 shows that in all the cases studied the maximum error is less than 5%.

Bifurcation Diagrams, Flow Patterns and Isotherms

The results of our computations will be presented in terms of bifurcation diagrams that show the conduction and convection solutions as a function of either the Rayleigh number (*Ra*) or the Frank-Kamenetskii (δ) parameter. Since each solution is characterized by the $2\times N\times M$ coefficients A_{ij} and B_{ij} $\{i=1,\ldots,M;\ j=1,2,\ldots,N\}$, a complete representation of the solutions requires a $2\times N\times(M+1)$ dimensional plot. The coefficients A_{ij} determine the nature of the flow pattern of a convective solution. If $A_{11}\neq 0$ while all other $A_{ij}=0$, then we have a one-roll solution. Similarly, if $A_{12}\neq 0$ and the rest $A_{ij}=0$, then a two-roll solution, and so on. These can be interpreted as pure modes predicted by the linear stability analysis. The solutions for which more than one $A_{ij}\neq 0$ may be interpreted as mixed-mode solutions. Positive and negative signs of A_{ij} correspond to different directions of rotation of the convective rolls. When there is only one layer of rolls in the vertical direction the coefficients A_{ij} $(i\geq 2)$ do not have any simple physical meaning and may be interpreted as the correction terms. The coefficients B_{i1} characterize the conduction solution while B_{ij} $(j\geq 2)$ characterize the convection branches. For a pure-mode m solution, $B_{im}\neq 0$, while all other B_{ij}'s $(j\neq 1,\ m)$ are zero.

Throughout this study, the convective solutions are described by using the square norm $\|\theta\|^2$ of the B_{ij} coefficients. This method of representation allows us to present a bifurcation diagram in a compact manner, but it cannot distinguish between positive and negative modes (characterized by the sign of A_{ij} coefficients or, equivalently, the direction of rotation of the rolls). Thus, separate bifurcation diagrams are presented for positive and negative modes.

It should be pointed out that unlike Lapwood convection that has up-down and left-right reflectional symmetry where the generators of the group are S_x and S_z (Impey et al., 1987), the system determined by Eqs. 55 and 56 with the boundary conditions of Eq. 57 does not have this symmetry. It is straightforward to show that this system has the symmetry given by

Table 1. Comparison of Numerically-Computed and Linear Stability Analysis ($\alpha=2$).

Mode No.	*Ra* (Linear Analysis)	*Ra* (Numerical)
1	15.381	15.250
2	21.739	22.250
3	36.539	37.500
4	44.400	45.000

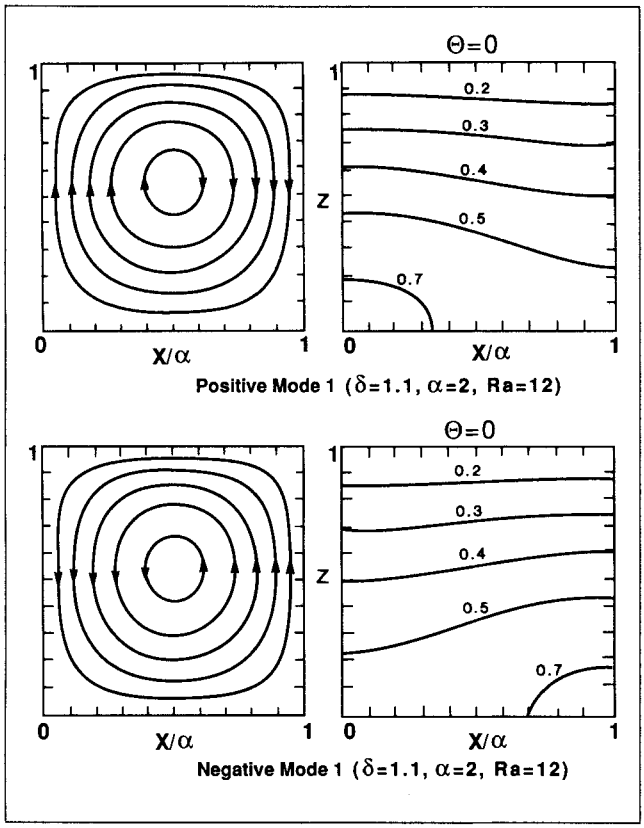

Figure 22. Streamlines and isotherms for positive and negative mode 1.

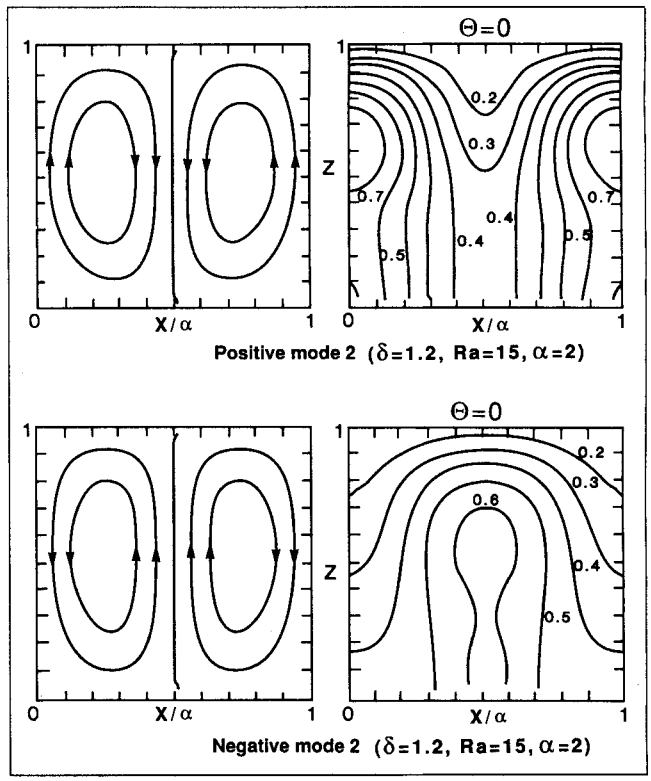

Figure 23. Streamlines and isotherms for positive and negative mode 2.

$$S_x(\Psi,\theta) = S_x[\Psi(x,z),\theta(x,z)]$$

$$= [-\Psi(-x,z), +\theta(-x,z)] \quad (60)$$

There is reflectional symmetry in the x direction, but not in the z direction. The question of symmetry arises when the meaning of the positive and negative solutions is studied. From a physical point of view, negative- and positive-mode solutions represent the same flow pattern, but the two solutions are mirror images of each other with the rolls rotating in opposite directions. When the isotherm plots are considered, two cases should be distinguished, odd- and even-mode solutions. The isotherm plots corresponding to positive and negative odd-mode solutions are mirror images of each other, while the isotherm plots corresponding to positive and negative even-mode solutions have the reflectional symmetry about the mid-plane $x=\alpha/2$. An example of this is shown in Figure 22 for positive and negative mode 1 and in Figure 23 for positive and negative mode 2. In both cases, the streamlines describe the same flow pattern but the rolls rotate in different directions. In the case of mode 2, the isotherms corresponding to the positive solution show two hot spots, one on each side of the domain, while those corresponding to negative mode 2 show only one hot spot in the central region of the box.

The stability behavior of the positive and the negative convective solutions can also be different for the case of even modes. A bifurcation diagram for positive and negative mode 2 is presented in Figure 24. The diagram for positive mode 2 (Figure 24a) shows that mode 1 (one-roll) is the first branching solution. Pure mode 2 solution bifurcates unstable from the conduction solution and changes stability after the merging point with the mode 1 solution. A stable secondary mode 2

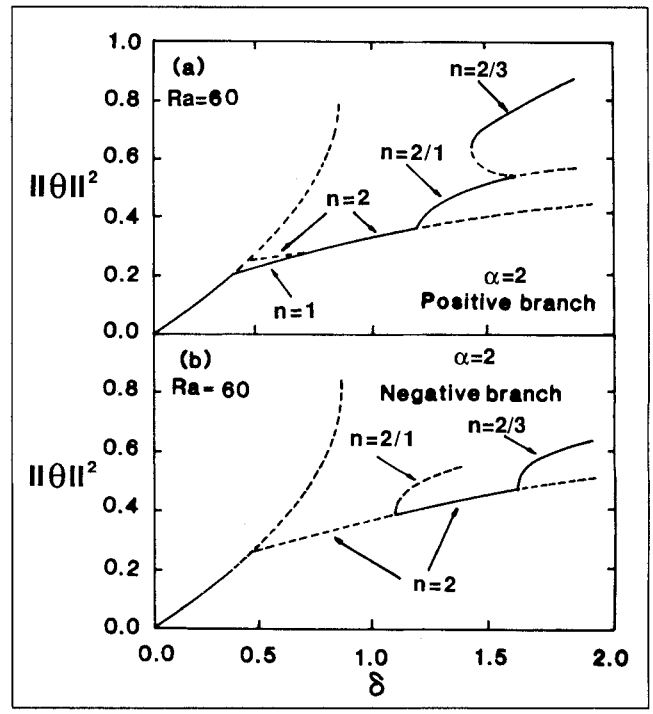

Figure 24. Bifurcation diagrams for mode 2: (a) positive branch; (b) negative branch.

solution appears at $\delta = 1.21$. This solution is a nonsymmetric two rolls solution that loses stability at $\delta = 1.61$ when an unstable tertiary bifurcation appears. This branch is a mixed 2/3 mode solution and is stable for $\delta > 1.42$. The bifurcation diagram for negative mode 2 is shown in Figure 24b. Pure mode 2 solution bifurcates unstable and changes stability after a secondary mixed mode 2/1 appears at $\delta = 1.13$. A secondary stable mixed 2/3 mode solution appears at $\delta = 1.63$. The pure mode 2 solution is unstable after the bifurcation of the stable mixed-mode solution.

The difference in the temperature distribution between stable and unstable convective solutions is shown in Figure 25 for modes 2 and 3. There is not a significant difference in flow patterns as a branch changes stability, for example, pure mode 2 branch in Figure 24b before and after the bifurcation of mixed 2/1 branch. However, differences can be found in the isotherms of the system before and after the change of stability. Stable mode 2 solutions have two hot spots on both corners of the domain (Figure 25a). As the system moves to higher δ values, the hot spots begin to move upward along the walls of the box and other hot spots slowly appear in the corners of the domain. The same behavior is found for mode 3 (Figure 25b). The stable branch has two hot spots on the bottom of the box. Those hot spots move upward along the walls and to the interior of the box as the δ values are increased. In both cases, the movement upward of the hot spots accompanies the change of stability. It should be pointed out that this behavior cannot be observed using lower-order approximations that involve only one term in the z direction. In the latter case, the hot spots will always appear on the bottom of the domain.

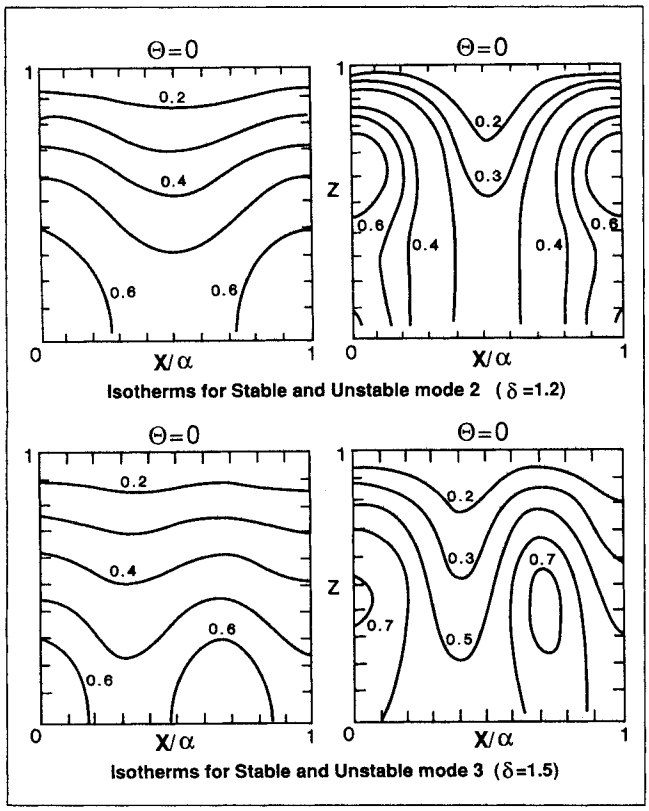

Figure 25. Isotherms for stable and unstable modes 2 and 3.

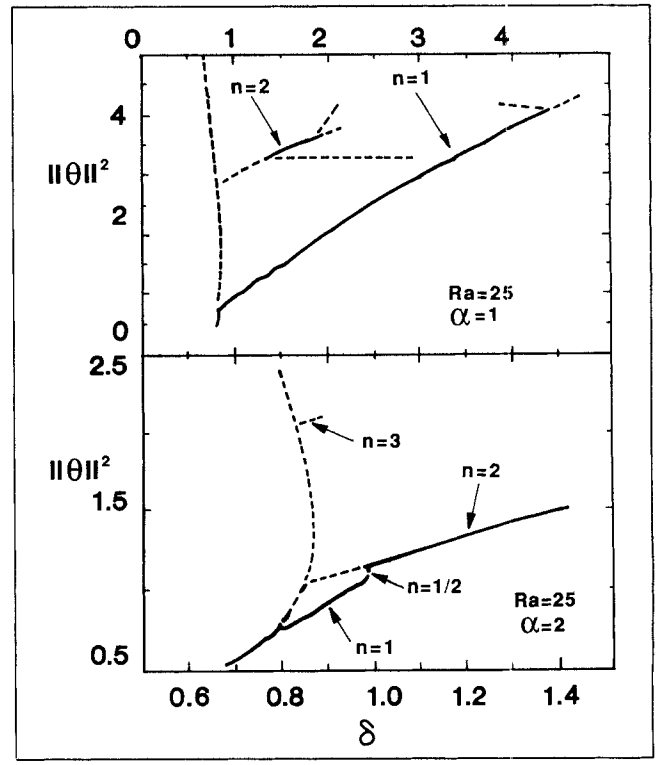

Figure 26. Bifurcation diagrams for $\alpha = 1$ and 2 (positive branches).

The evolution of the bifurcation diagram as the value of α is increased is shown in Figures 26 and 27. For the sake of simplicity, only the principal positive branches are shown. For

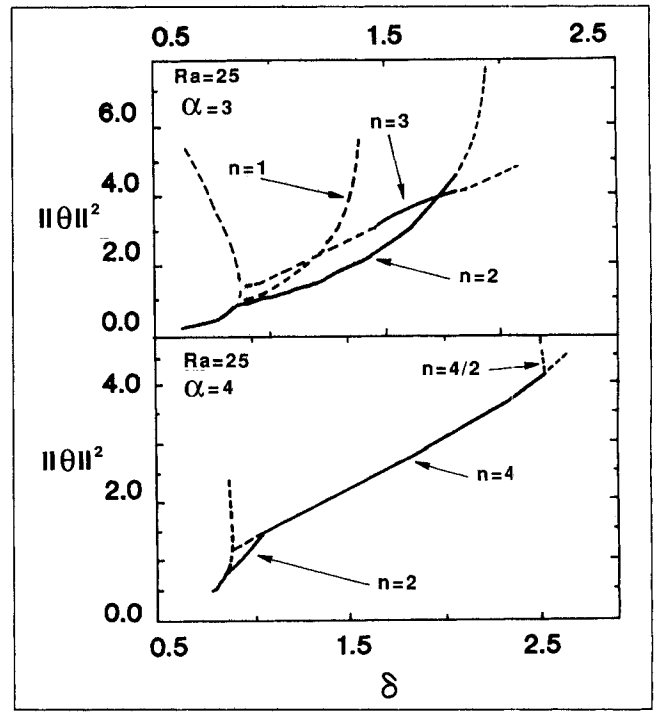

Figure 27. Bifurcation diagrams for $\alpha = 3$ and 4 (positive branches).

$\alpha = 1$, the most important branches are modes 1 and 2. A connection between these two solutions was not found within the range of δ shown in Figure 26. For $\alpha = 2$, modes 1 and 2 are also the most important modes, but they are connected by a mixed 1/2-mode branch. The principal modes for $\alpha = 3$ are 1, 2 and 3. For this particular set of parameter values ($Ra = 25$), mode 2 is the first branch bifurcating from the lower conduction solution. Numerical calculations showed that for $\alpha = 3$, the bicritical point of modes 1 and 2 is located at $Ra = 20.7$. Thus, for $Ra = 25$, mode 2 becomes the first branch bifurcating from the lower conduction solution. This numerically-determined value of the Rayleigh number at which the change occurs is in good agreement with the exact value calculated from linear analysis ($Ra = 21.2$). For $\alpha = 4$ and $Ra = 25$, mode 2 is also the first branch bifurcating from the conduction solution. Mode 2 solution is connected to mode 4 solution through a mixed 2/4 branch that cannot be seen in the figure. Mode 4 solution changes stability after the merging point with the mixed 2/4 branch and is the stable solution at high δ values. This behavior involving modes 2 and 4 is similar to what happens with modes 1 and 2 in Figure 26. Figures 26 and 27 clearly show the effect of the aspect ratio on the type of convection solution that exists inside the system. In this case, a one-roll solution that exists for $\alpha = 1$ changes to a stable four rolls solution for $\alpha = 4$ at higher values of the Frank-Kamenetskii parameter.

Another way to look at the behavior of the system is using bifurcation diagrams that take the Rayleigh number as the distinguished parameter. This kind of graphs allows one to study precisely the relative position of the different branches and mode interactions for a fixed δ value. They may also be used to check the accuracy of the numerical solutions close to the conduction branch. Figure 28 shows a bifurcation diagram for $\delta = 0.8$ and $\alpha = 3$. The values of the Rayleigh number, where the different branches bifurcates from the conduction solution may be found by the linear analysis in Part I. Once again, good agreement was found between the numerically-computed and the linear analysis results. Mode 2 is the first branch bifurcating stable from the conduction solution and mode 3 is the second. The presence of a stable mixed 3/2 solution is also observed. This branch will eventually become a two-roll solution. The different behavior of positive and negative solutions can be seen in Figure 29 for $\delta = 0.7$ and $\alpha = 4$. Mode 3 is the first branch bifurcating stable (both positive and negative branches), and modes 4 and 2 are the second and third bifurcating solutions, respectively. As mentioned previously, positive and negative mode 4 and 2 branches have different stability behavior. In the bifurcation diagram for positive solutions, mode 2 and 4 branches are connected to each other, while negative mode 2 and 4 solutions are not. Modes 1 and 5 are connected by a mixed 1/5 mode branch.

Bifurcation diagrams that use δ as distinguished parameter allow one to study the stability of the system as the heat generation (δ) is increased. Figures 27a, 30, 31, 32 and 33 show the evolution of the bifurcation diagram as Ra is increased, for positive and negative modes and a fixed aspect ratio ($\alpha = 3$). The stability of the different solutions is also shown in these figures. Note that for the case of $Ra = 0$, only the conduction solutions exist as shown in Figure 1b. For small, but nonzero, values of Ra, unstable convective solutions branch off the middle conduction solution as shown in Figure 30a. The convective solution that is closest to the limit point is always mode

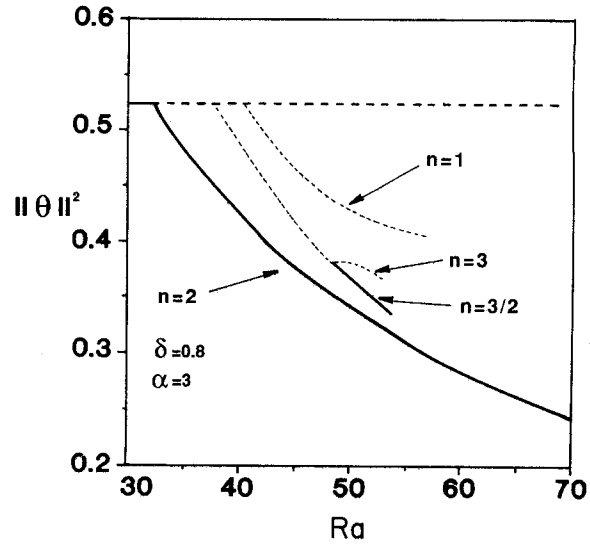

Figure 28. Bifurcation diagram for $\delta = 0.8$ with Ra as the bifurcation parameter.

1 for all aspect ratios. For $Ra > Ra'$ (≈ 8.5 for $\alpha = 3$), mode-1 solution becomes stable through a Hopf bifurcation and loses stability again by a limit-point bifurcation (Figure 30b). For $Ra > Ra^*$ (≈ 9.0 for $\alpha = 3$), the stable mode 1 branch overlaps with the conduction solution as shown in Figure 30c. This bifurcation behavior persists until $Ra = 14.2$ at which mode 1 crosses the limit point. It is interesting to note that for $Ra' < Ra < Ra^*$, a stable convective solution exists but explo-

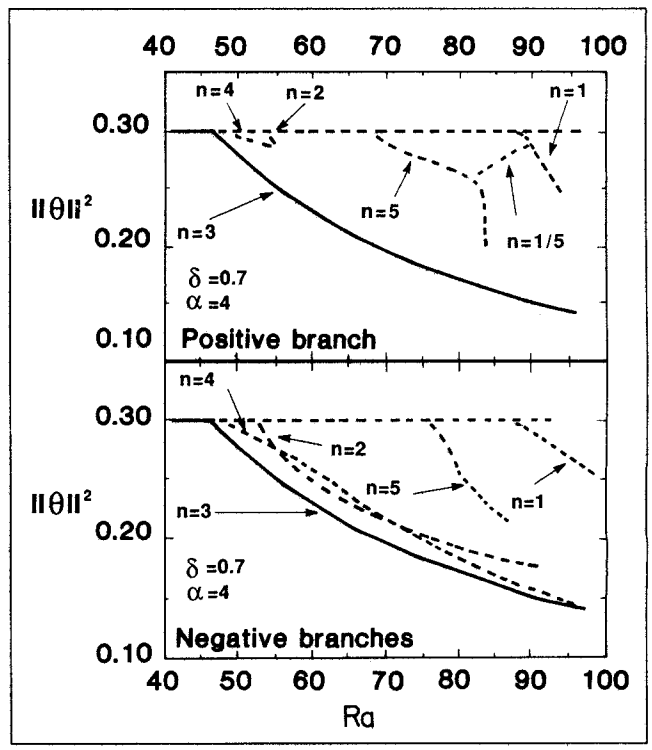

Figure 29. Bifurcation diagram of positive and negative branches for $\delta = 0.7$ with Ra as the bifurcation parameter.

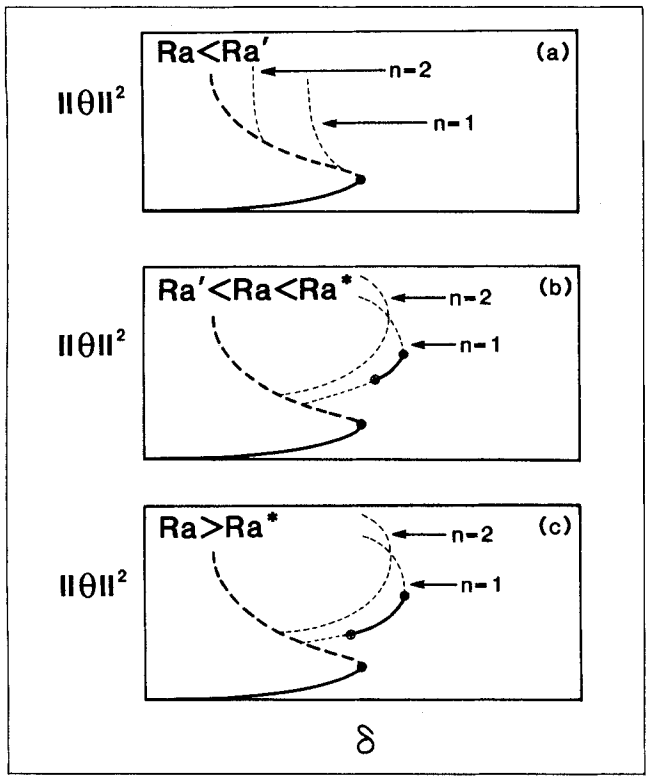

Figure 30. Bifurcation diagrams of positive branches of convective solutions for $\alpha = 3$ at small values of Rayleigh number.

•, limit point; ⊗, Hopf bifurcation point.

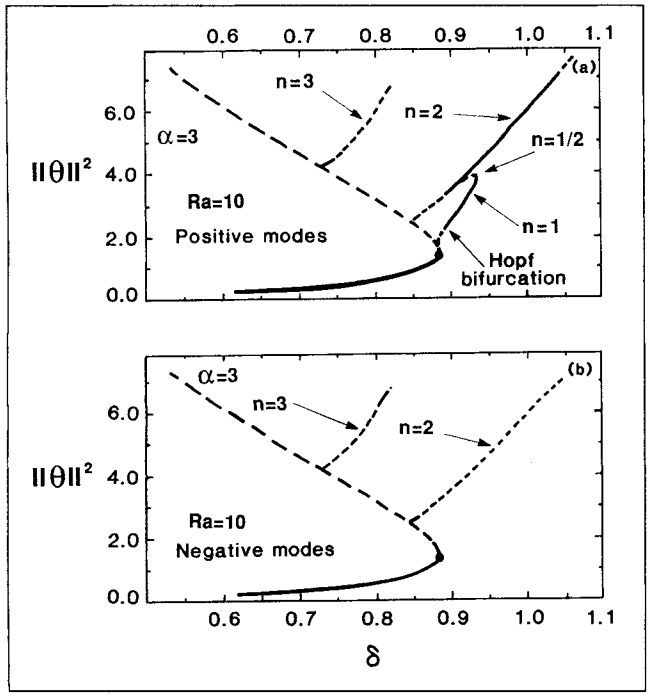

Figure 31. Bifurcation diagrams for $\alpha = 3$, positive and negative branches for $Ra = 10$ (• limit point).

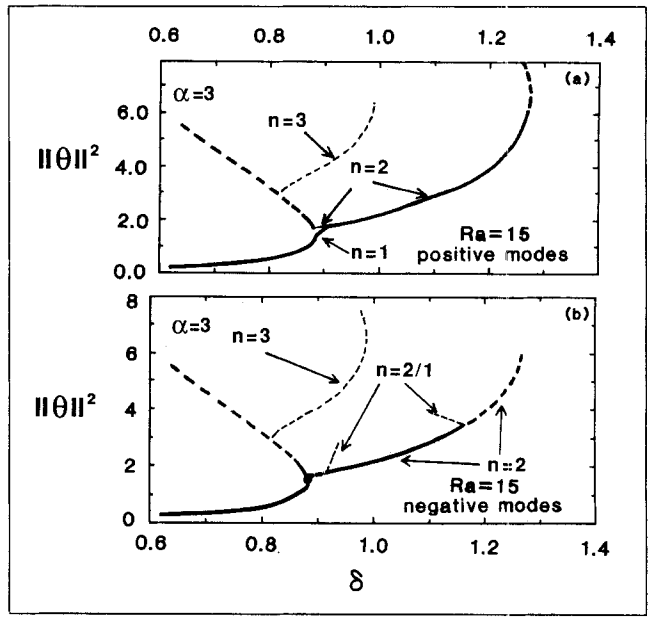

Figure 32. Bifurcation diagrams for $\alpha = 3$, positive and negative branches for $Ra = 15$ (• limit point).

sion still occurs at the conduction limit. Only for $Ra > Ra^*$, the convective solution extends the explosion limit. This limit is further extended by the mode 2 convective branch (Figure 19a).

For Ra values greater than 14.2, mode 1 solution bifurcates as a stable branch from the lower conduction solution. This branch becomes unstable to a mixed mode 1/2 solution which connects it to a stable mode 2 branch (Figures 31a and 32a). Mode two solution crosses into the lower conduction solution at $Ra = 20$. Both branches switch positions at $Ra = 20.7$ and

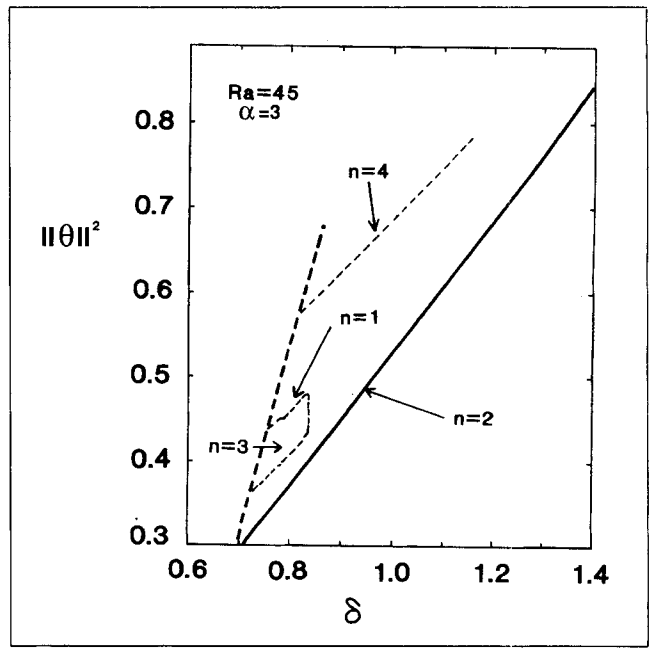

Figure 33. Bifurcation diagram of convective solutions for $Ra = 45$ and $\alpha = 3$.

then mode 2 is the first convective solution bifurcating stable from the conduction solution (Figure 27a). Modes 1 and 3 interchange positions at $Ra = 32.5$. For the values of Ra exceeding this number, mode 3 is the second bifurcating solution. For higher Ra numbers, modes 1 and 3 are connected through a 3/1 mixed-mode solution (Figure 33). The bifurcations diagrams for the negative modes (Figures 31b and 32b) have many differences compared to the equivalent diagrams for positive modes. Both mode 1 branches (positive and negative) join the positive mode 2 solution. That is the reason why they do not appear in the plots for negative branches. Positive and negative mode 2 solutions coincide in a $\|\theta\|^2$ vs. δ diagram, but the stability of both branches is different. Positive mode 2 branch changes stability after the merging with the positive and negative mode 1 branches. However, as shown in Figure 31b, the stability of negative mode 2 does not change. Figure 32b shows that the stability of this branch changes only after the bifurcation of a mixed mode 2/1 solution.

As Ra number increases, mode 1 branch moves along the conduction solution at a rate that is lower than the other modes. So, as Ra number is increased mode 1 solution will interchange positions first with mode 2, then with mode 3 and so forth. Just after the crossing both branches are connected by a mixed-mode solution, for example, 1/3 in Figure 33. The bifurcation sequence shown in Figures 30 to 33 is found to be qualitatively the same for other aspect ratios ($\alpha = 1$, 2 and 4). The extension of the calculations to higher Ra numbers was not pursued due to the presence of many convective branches and the mixed-mode branches connecting them.

Determination of the Ignition Point in the Presence of Natural Convection

The main practical importance of convective solutions is to increase the stability of the system. The convective movement increases the heat removal, allowing to have a safe system for heat generation rates much higher than the ones predicted using only a conductive solution. In Figure 34, the critical Frank-Kamenetskii number, the δ value beyond which there is not any stable branch (conduction or convection), is plotted vs. the Ra number for $\alpha = 1, 2$ and 3. The absence of stable branches means that an explosion will occur in the system. Each curve in Figure 34 was constructed gathering information from a set of bifurcation diagrams having the same α value and different Ra numbers. It was shown in Figures 30, 31, 32 and 33 that as the Ra number is increased, the system passes through different convective states that produce the discontinuities in different curves. For example, the ignition locus for $\alpha = 3$ has three segments within the range of Rayleigh numbers studied. First, the critical value is given by the conduction solution up to $Ra = 9$ ($\delta_{ig} = 0.8785$). Mode 1 branch is the first convective solution that expands the stability range beyond the conduction limit up to $Ra = 24$. Then, mode 2 is the solution branch that extends the stability range to even higher δ values. These convective states are shown in Figure 34. As mentioned above, the extension of this figure for Ra values beyond the range used here is complicated because of the numerous convective solutions present.

By comparing the curves in Figure 34 for different α values, we can say that for a given Ra number the critical Frank-Kamenetskii number (δ_c) decreases as the width is increased.

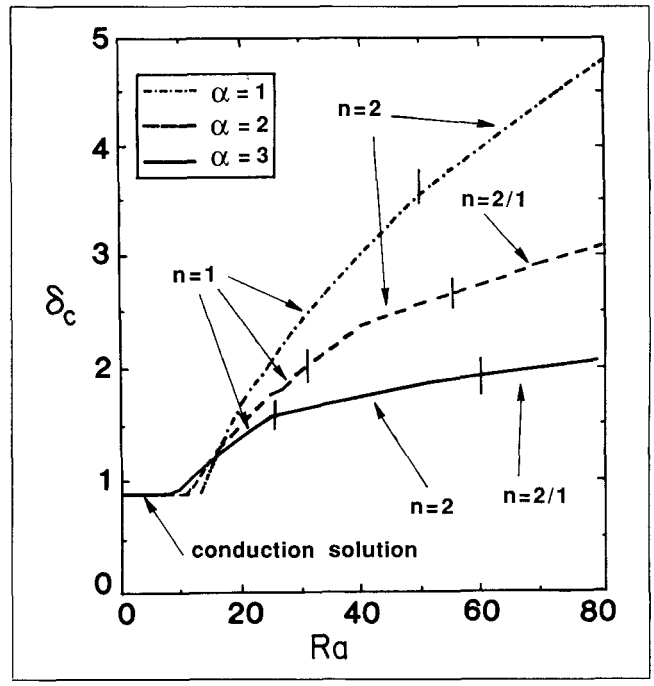

Figure 34. Dependence of the critical Frank-Kamenetskii number, δ_c (explosion limit) on the Rayleigh number for $\alpha = 1$, 2 and 3.

The square box ($\alpha = 1$) is the safest, then $\alpha = 2$, and so on. It can also be seen from Figure 34 that for a given Ra number, the number of rolls in the three possible configurations of the box are approximately the same. This means that for a given number of rolls (circulations), the heat removal increases as the width decreases. For any aspect ratio, natural convection increases the explosion limit several times beyond the conduction limit (more than five times for $\alpha = 1$).

Conclusions and Remarks

In Part I of this work, we have examined the onset of reaction-driven convection in a porous medium using linear stability analysis. The analysis presented here is quite general and includes two-dimensional as well as three-dimensional disturbances. We have determined the critical Rayleigh number (Ra_{min}) and the wave number (k_{min}) as a function of the reaction parameters. For the case of insulated bottom boundary condition (box), it was found that Ra_{min} and k_{min} decrease monotonically to zero as the Frank-Kamenetskii parameter (δ) increases to the value corresponding to that at the limit point of the conduction solution. This result implies that for the insulated bottom case, convection could set in at arbitrarily small values of the Rayleigh number, provided that the value of δ is close to that at the ignition point. In contrast, for the case of fixed-temperature boundary conditions (cylinder), Ra_{min} and k_{min} do not approach zero as δ approaches the value corresponding to that at the ignition point of the conduction branch. Thus, for the case of fixed-temperature boundary conditions, the Rayleigh number must exceed a certain critical value before the lower conduction branch becomes unstable to convective disturbances.

Our analysis has shown that two types of mode interactions are important in the case of reaction-driven convection: the interaction of a convective mode with a limit point of the conduction solution and the interaction of two convective modes. Figure 6 gives the locus of parameter values at which the first type of interaction occurs for the case of $\gamma=\infty$. For the case of a box, as the Rayleigh number is increased the wave number also increases. Thus, the first mode to cross the limit point to the lower conduction branch has the smallest k value ($n=0$, $m=1$, if $\alpha_1>\alpha_2$ or $n=1$, $m=0$, otherwise). As the Rayleigh number is increased further, convective modes interact and the flow patterns are more complicated. For the case of a cylinder, Figure 6 shows that as Ra is increased, the first convective mode to move to the lower conduction branch may be either two- or three-dimensional depending on the aspect ratio. Figure 17 shows that for a cylinder with equal height and diameter, the flow pattern is three-dimensional and not axisymmetric. Thus, the results of Kordylewski and Krajewski (1984) for the determination of the ignition point on the Rayleigh number are not correct.

In Part II of this work, we presented a systematic numerical study of reaction-driven convection in a two-dimensional box. The different types of convective solutions are determined as a function of the Rayleigh number, Frank-Kamenetskii parameter and aspect ratio. It was shown that lower-order numerical approximations may fail to capture qualitative details of the bifurcation picture.

It was found that negative and positive convective modes have similar flow patterns with rolls rotating in opposite directions. The isotherms for negative and positive odd-mode solutions are mirror images of each other. On the other hand, for even modes the isotherms for negative and positive solutions show different numbers of hot spots. Negative and positive branches of even-mode solutions were found to have different stability behavior. The loss of stability of a convective solution is associated with the movement upward of the hot spots.

For some typical aspect ratios, we determined the different bifurcations diagrams, and the number and order of stable convective solutions. It was found that many stable convective solutions can appear, depending on the value of the system parameters. For any fixed Ra, there exists a critical Frank-Kamenetskii number beyond which no stable (conduction or convection) solution exists. We determined this ignition limit for three typical aspect ratios.

The calculations showed that the heat removal improves for small aspect ratios. Natural convection extends the ignition (explosion) limit of the system several times beyond the conduction limit.

Acknowledgment

We are grateful to the American Chemical Society Petroleum Research Fund (ACS-PRF) the Texas Advanced Research Program and the Robert A. Welch Foundation for support of this study.

Notation

A = $\rho_m C_{pm}/\rho_f C_{pf}$
a = radius of cylinder or width of rectangle
b = breadth of rectangle
C_{pf} = fluid phase heat capacity
C_{pm} = porous medium heat capacity
c_0 = reactant concentration
E = activation energy
g = acceleration due to gravity
h = half-height of cylinder or height of rectangle
ΔH = heat of reaction
K = permeability
k = wave number
k_e = effective thermal conductivity
k_0 = pre-exponential kinetic factor
n = outer normal
P = dimensionless pressure $PK\rho_f C_{pf}/\mu k_e$
R = universal gas constant
Ra = Rayleigh number $\beta g T_0 hK/\nu\kappa\gamma$
T_0 = ambient temperature
U = dimensionless velocity $U\rho_f C_{pf} h/k_e$
u, v, w = z-dependent parts of disturbance velocity eigenfunctions

Greek letters

α_1, α_2 = x and y aspect ratios for rectangle, a/h, b/h
α = aspect ratio for two-dimensional box, a/h
β = coefficient of fluid thermal expansion
γ = dimensionless activation energy, E/RT_0
δ = Frank-Kamenetskii parameter, $(-\Delta H)c_0 h^2\gamma k_0 \exp(-\gamma)/k_e T_0$
η = aspect ratio of cylinder, a/h
κ = effective thermal diffusivity $k_e/\rho_f C_{pf}$
ζ = eigenvalue for quiescent solution
λ = eigenvalue for convective solution
θ = dimensionless temperature $\gamma(T-T_0)/T_0$
ν = kinematic viscosity μ/ρ_f
Π = disturbance pressure eigenfunction
ρ_f = fluid density
ρ_m = medium density
μ = fluid viscosity
Θ = disturbance temperature eigenfunction
ϕ = z-dependent part of disturbance temperature eigenfunction
ψ = azimuthal angle in cylindrical polar coordinates
Ψ = stream function

Subscripts

c = critical
e = effective
f = fluid
i = ignition
o = reference state

Literature Cited

Abramowitz, M., and I. A. Stegun, *Handbook of Mathematical Functions*, Dover publications, New York (1965).

Armbruster, D., J. Guckenheimer, and P. Holmes, "Heteroclinic cycles and Modulated Traveling Waves in Systems with O(2) Symmetry," *Physica D*, **29**, 257 (1988).

Beck, J. L., "Convection in a Box of Porous Material Saturated with Fluid," *Phys. Fluids*, **15**, 1377 (1972).

Coddington, E. A., and N. Levinson, *Theory of Ordinary Differential Equations*, McGraw-Hill, New York (1955).

Dangelmayr, G., and D. Armbruster, "Steady State Mode Interactions in the Presence of O(2) Symmetry and in Non-Flux Boundary Value Problems," *Multiparameter Bifurcation Theory*, M. Golubitsky and J. Guckenheimer, eds., Amer. Mathematical Soc. (1986).

Davis, S. H., "Convection in a Box: Linear Theory," *J. Fluid Mech.*, **30**, 465 (1967).

Frank-Kamenetskii, D. A., *Diffusion and Heat Transfer in Chemical Kinetics*, 2nd ed., Plenum, New York (1969).

Gatica, J. E., H. J. Viljoen, and V. Hlavacek, "Interaction between Chemical Reaction and Natural Convection in Porous Media," *Chem. Eng. Sci.*, **44**(9), 1853 (1989).

Gershuni, G. Z., and E. M. Zhukovitskii, *Convective Stability of Incompressible Fluids*, Israel Program for Scientific Translations, Jerusalem (1976).
Golubitsky, M., and D. G. Schaeffer, *Singularities and Groups in Bifurcation Theory*, Vol. I, Springer-Verlag, New York (1985).
Golubitsky, M., I. Stewart, and D. G. Schaeffer, *Singularities and Groups in Bifurcation Theory*, Vol. II, Springer-Verlag, New York (1988).
Guckenheimer, J., and Holmes, P. J., *Nonlinear Oscillations, Dynamical Systems, and Bifurcations of Vector Fields*, Springer-Verlag, New York (1983).
Homsy, G. M., and A. E. Sherwood, "Convective Instabilities in Porous Media with Through Flow," *AIChE J.*, **22**, 168 (1976).
Impey, M. D., D. S. Riley, and K. H. Winters, "The Effect of Sidewall Imperfections on Pattern Formation in Lapwood Convection," *Bifurcation Phenomena in Thermal Processes and Convection*, HTD-Vol. 94, AMD-Vol. 89, p. 99, H. H. Bau, ed., ASME (Dec., 1987).
Jones, D. R., "The Dynamic Stability of Confined, Exothermically Reacting Fluids," *Int. J. Heat and Mass Transfer*, **16** 157 (1973).
Jones, M. C., and J. M. Persichetti, "Convective Instability in Packed Beds with Through Flow," *AIChE J.*, **32**, 1555 (1986).
Kordylewski, W., and Z. Krajewski, "Convection Effects on Thermal Ignition in Porous Media," *Chem. Eng. Sci.*, **39**, 610 (1984).
Kordylewski, W., B. Borkowska-Pawlik, and J. Slany, "Stability of Three-Dimensional Natural Convection in a Porous Layer," *Arch. Mech.*, **4**, 383 (1986).
Kubicek, M., and M. Marek, *Computational Methods in Bifurcation Theory and Dissipative Structure*, Springer-Verlag, New York (1983).
Lapwood, E. R., "Convection of Fluids in Porous Media," *Proc. Camb. Phil. Soc.*, **44**, 508 (1948).
Nield, D. A., "Onset of Thermohaline Convection in a Porous Medium," *Water Resources Res.*, **4**, 553 (1968).
Viljoen, H., and V. Hlavacek, "Chemically Driven Convection in a Porous Medium," *AIChE J.*, **33**, 1344 (1987).

Manuscript received Dec. 4, 1990, and revision received Mar. 21, 1991.